Original research

Faecal microbial transfer and complex carbohydrates mediate protection against COPD

9,10 Nancy Lachner, Sobia Idrees © 3.4 Saima Firdous Rehman © 1.3.4 Alen Faiz © 7 Vyoma K Patel, 3.4 Chantal Donovan © 1.4 Charlotte A Alemao, 1 Sj Shen © 3.4 Nadia Amorim © 3.4 Rajib Majumder © 3.4 Kanth S Vanka © 1 Jazz Mason, 1 Tatt Jhong Haw © 1 Bree Tillet © 8 Michael Fricker © 1 Simon Keely © 1 Nicole Hansbro © 3.4 Gabrielle T Belz © 8 Jay Horvat © 1 Thomas Ashhurst © 9.7 Nicole Hansbro © 9.11 Helen McGuire © 1 Barbara Fazekas de St Groth © 11 Nicholas J C King © 9.10,11,12 Ben Crossett © 13 Stuart J Cordwell © 13,14 Nicholas J C Ring © 15.16 Inarhim I Schultze © 15,16,17 9′9 (a) Nicholas J C King © '9,10,11,12 Ben Crossett © '13 Stuart J Cordwell © '13,14 Lorenzo Bonaguro © '15,16 Joachim L Schultze © '15,16,17 Emma E Hamilton-Williams © '8 Elizabeth Mann, ¹⁸ Samuel C Forster © '19 Matthew A Cooper © '20 Leopoldo N Segal © '21 Sanjay H Chotirmall, ²² Peter Collins © '23,24 Rayleen Bowman, ^{5,6} Kwun M Fong © '5,6 Ian A Yang Peter A B Wark © '1 Paul G Dennis © '25 Philip Hugenholtz © '2 Kurtis F Budden 🆁 ,¹ Shakti D Shukla 🕲 ,¹ Kate L Bowerman 🕲 ,² Annalicia Vaughan 🕲 ,³,4,5,6 Shaan L Gellatly 🕲 ,¹ David L A Wood 🔞 ,²

► Additional supplemental material is published online only. To view, please visit the journal online (https://doi.org/10.1136/gutjnl-2023-330521).

For numbered affiliations see end of article.

Correspondence to

Professor Philip M Hansbro, Centenary Institute and University of Technology Sydney, Sydney, NSW, Australia; Philip:Hansbro@uts.edu.au

KFB, SDS and KLB contributed equally.

KFB, SDS and KLB are joint first authors.

Received 18 June 2023 Accepted 8 January 2024 Published Online First 8 February 2024



© Author(s) (or their employer(s)) 2024. No commercial re-use. See rights and permissions. Published by BMJ.

To cite: Budden KF, Shukla SD, Bowerman KL, et al. Gut 2024;**73**:751–769.

supplementation of mice or human patients with complex

carbohydrates improved disease outcomes.

metabolomics identified downregulation of glucose and

starch metabolism in CS-associated microbiota, and

and *Lachnospiraceae* family members. Proteomics and

NBSTRACT

Objective Chronic obstructive pulmonary disease (COPD) is a major cause of global illness and death, most commonly caused by cigarette smoke. The mechanisms of pathogenesis remain poorly understood, limiting the development of effective therapies. The gastrointestinal microbiome has been implicated in chronic lung diseases via the gut-lung axis, but its role is undear.

absence of CS exposure. Disease features correlated with the were assessed in mice using a high resistant starch diet, and in 16 patients with COPD using a randomised, double-blind, transfer of CS-associated microbiota after antibiotic-induced relative abundance of Muribaculaceae, Desulfovibrionaceae (inflammation, alveolar destruction, impaired lung function), (CS)-induced COPD and faecal microbial transfer (FMT), we Design Using an in vivo mouse model of cigarette smoke histopathology and lung function. Complex carbohydrates gastrointestinal pathology and systemic immune changes. Protective effects were additive to smoking cessation, and characterised the faecal microbiota using metagenomics, placebo-controlled pilot study of inulin supplementation. proteomics and metabolomics. Findings were correlated inflammation while suppressing colonic immunity in the with airway and systemic inflammation, lung and gut microbiome depletion was sufficient to increase lung Results FMT alleviated hallmark features of COPD

WHAT IS ALREADY KNOWN ON THIS TOPIC

⇒ Changes in gut microbiota are associated with chronic obstructive pulmonary disease (COPD) but the underlying host and microbial mechanisms are unclear, limiting the therapeutic applications.

WHAT THIS STUDY ADDS

- ⇒ Microbiome composition and metabolism is reproducibly correlated with lung and gastrointestinal pathology in experimental COPD.
 - Microbiome modifying interventions effectively alleviate disease, including protective effects supplementing smoking cessation.
- ⇒ Lung and colonic immune changes can be induced by transfer of microbiota from mice with experimental COPD into naïve
- recipients.
 ⇒ Nutritional interventions targeting the microbiome in patients with COPD demonstrate efficacy in a small pilot study.

HOW THIS STUDY MIGHT AFFECT RESEARCH, PRACTICE OR POLICY

⇒ Microbiome-targeting therapeutics and nutritional interventions may be developed for COPD, including as supplements to smoking cessation. **Conclusion** The gut microbiome contributes to COPD pathogenesis and can be targeted therapeutically.

Chronic obstructive pulmonary disease (COPD) is most often caused by long-term cigarette smoke (CS) inhalation and includes chronic inflammation, airway remodelling and emphysema leading to progressive lung function impairment which persists after smoking cessation. Over 210 million people globally have COPD, causing >3.3 million deaths annually although even these are substantially under-reported. Pharmacological treatments have little efficacy in reversing disease, suppressing its progression or preventing mortality and have significant adverse effects. Mechanisms of COPD pathogenesis remain poorly understood and no singular driver of disease has been discovered, suggesting that chronic effects from a range of factors drive disease pathogenesis over many years. Development of effective therapies will require targeting this array of factors.

The microbiome is under intense investigation for its immunoregulatory capacity and association with disease. Most COPD studies have focused on respiratory microbiota, demonstrating increased bioburden, reduced diversity and enrichment of *Firmicutes* and *Proteobacteria*.

The gut hosts the largest and most diverse microbiome of the human body that, depending on its composition, can drive or suppress inflammation, including in the lung.⁶ Alterations in the gut microbiome from antibiotics or diet influence asthma development and respiratory infections.⁶ Chronic CS-exposure induces gastrointestinal histopathology,⁷ and patients with COPD have increased risk of inflammatory bowel diseases⁶ and altered gut microbiome composition.⁸

Transfer of whole microbial communities from healthy individuals through faecal microbial transfer (FMT) is an effective therapy in patients with Clostridioides difficile colitis, but its implementation in other diseases is not as well supported. FMT may therefore have cost-effective benefits in COPD, but further examination is required. A study using a short-term smoke and poly I:C (TLR3 agonist) model showed that FMT prevented emphysema and identified associations with Bacteroidaceae and Lachnospiraceae families by 16S rRNA gene sequencing, 10 but important controls and analyses linking taxa to pathogenesis were lacking and the model was not representative of human CS-induced COPD. Similarly, Parabacteroides goldsteinii lipopolysaccharide (LPS) had protective effects in a murine model of COPD, but broader associations between microbiota and disease were not identified.¹¹ Crucially, neither study identified bacteria associated with COPD in human studies⁸ or demonstrated human translation.

We hypothesised that gastrointestinal microbiota contribute to COPD pathogenesis, and provide a detailed characterisation of the gastrointestinal microbiome in experimental CS-induced COPD using multiomics. FMT protected against experimental COPD through changes in microbiota that correlated with key disease features. Proteomics and metabolomics implicated restoration of bacterial complex carbohydrate metabolism in the protective effects, supported by interventional studies in experimental COPD and human patients with COPD.

METHODS

Mice, CS-exposure, microbiome transfer and diet studies

Female C57BL/6 mice (3–5 weeks old) from the University of Newcastle Animal Service Unit (Newcastle, Australia) underwent 3 weeks of baseline microbiome normalisation

by transferring soiled bedding and co-housing. Microbiome normalisation was not performed for validation experiments (8 weeks CS).

Mice were exposed to normal room air or CS from 12 3R4F cigarettes (University of Kentucky, Lexington, Kentucky, USA) twice per day, 5 days per week, for 8 or 12 weeks as previously described. 12-20 FMT was administered twice per week by transfer of soiled bedding or oral gavage of faecal supernatants from agematched air-exposed mice to CS-exposed mice and vice versa (online supplemental figure S1). Experimental controls were used as donors for the FMT to ensure the use of age-matched donors which had undergone microbiome normalisation, minimising variability and confounding factors (online supplemental figure S1).

For antibiotic depletion experiments, mice received antibiotics (ampicillin, metronidazole, neomycin, gentamicin (1g/L) and vancomycin (0.5 g/L)) in drinking water for 7 days. ²¹ Antibiotics were removed and mice received FMT from a separate cohort of air-exposed or CS-exposed donors four times in 10 days. FMT recipient mice were not exposed to CS directly. For diet studies, mice were fed a conventional semi-pure diet (AIN93G) or a resistant starch diet (SF11-025; Specialty Feeds, WA, Australia) ad libitum commencing 2-week prior to CS-exposure and maintained until the end of experiment. Faeces were collected weekly, with at least three fresh faecal pellets collected and stored at -80°C until processing. Airway inflammation, lung and colon histopathology, lung function and gene expression analyses were assessed as previously described. ⁷ ¹²⁻²⁰ ²² Detailed methods are provided in the online supplemental file 1.

All experiments were approved by University of Newcastle Animal Ethics Committee.

Analysis of gut microbiome

Faecal microbiome composition, including metagenomics and 16S rRNA gene sequencing, were analysed as previously described⁸ with detailed methods provided in the online supplemental file 1. Briefly, α-diversity was calculated using QIIME V.1.8.0,²³ principal component analysis performed using the R package vegan V.2.5-1²⁴ within metagenomeSeq V.1.22.0²⁵ and differential abundance determined using DESeq2 with Benjamini-Hochberg adjustment. Sparse Partial Least-Squares Discriminant Analysis (sPLS-DA) was conducted using the R package mixOmics V.6.3.2.²⁶ Host phenotypes were tested for association with microbiome composition using the envfit function within the vegan R package. Spearman's rho was calculated using the 'corr.test' function within the R package psych V.1.8.12.²⁷ Non-random relationships between taxa were assessed using the CoNET Cytoscape application.²⁸

Cytometry by time-of-flight analysis

For time-of-flight mass cytometry, single cell suspensions of bone marrow, blood and spleen cells were stained with cell cycle marker iododeoxyuridine (IdU), viability marker cisplatin and surface and intracellular antibodies (online supplemental table S19). Expression levels of 38 markers were measured using a Helios instrument (Fluidigm), transformed with a logicle transformation²⁹ and used for Uniform Manifold Approximation and Projection for Dimension Reduction (UMAP) using the naïve R implementation (umap V.0.2.7). Cells clusters were calculated using Rphenograph (Github JinmiaoChenLab V.0.99.1).³⁰ Detailed methods are provided in the online supplemental file 1.

Cell culture

Raw 264.7 monocytes (1×10^6) were seeded into 12-well plates. Cells were incubated in media alone, or 1:1000 dilutions of sterile-filtered faecal homogenate ($100\,\text{mg/mL}$) from CS-exposed or air-exposed mice for 24 hours. During the final 4 hours, LPS ($1\,\mu\text{g/mL}$), monophosphoryl lipid A ($4\,\mu\text{g/mL}$), lipoteichoic acid ($1\,\mu\text{g/mL}$) were added to cell media. Tumour necrosis factor (TNF)- α protein in culture media was assessed using DuoSet ELISA kits (R&D Systems).

Flow cytometry

Colon²¹ and lung tissue¹³ ¹⁸ were digested to produce single cell suspensions and stained for flow cytometry as previously described, before analysis using an LSRFortessa cytometer (BD Biosciences) and FlowJo software (TreeStar). Details are provided in the online supplemental file 1.

Proteomics of mouse faeces

Faecal proteins were analysed by nanoflow liquid chromatography (Ultimate 3000 RSLCnano, Thermo Scientific) with peptides introduced via an Easy-Spray Nano source coupled to a Q-Exactive Plus Quadrupole Orbitrap mass spectrometer (Thermo Scientific) and subjected to data dependent tandem mass spectrometry (MS/MS). Raw files were processed in Proteome Discoverer V.2.1 using the Sequest HT algorithm,³¹ searched against the mouse gut microbiota GigaDB database³² and integrated with metagenomics results using the psych package in R³³ and Diablo mixOmics package. Detailed methods are provided in the online supplemental file 1.

Metabolomics

Metabolomics of caecum contents was performed by Metabolon (Durham, North Carolina, USA) using the Global HD4 MS platform as previously described. Detailed methods are provided in the online supplemental file 1.

Human interventional study

Sixteen patients with COPD were recruited from June 2019 to March 2020 at the Respiratory Investigation Unit at The Prince Charles Hospital (TPCH) with written and informed consent. Nine participants were randomised into the intervention arm (inulin 10 g daily for 4 weeks) and seven to the placebo group (maltodextrin 10 g daily for 4 weeks). Age, gender, body mass index (BMI), smoking history (pack years) and spirometry (forced expiratory volume in 1s/ forced vital capacity (FEV1) and FEV1% predicted) were similar between the two groups (table 1).

Statistical analysis

Except where specified, data was analysed in GraphPad Prism V.9.0 (San Diego, California, USA). Outliers were identified by Grubbs test, and excluded from analysis only if investigators had reported technical errors during sample collection/processing before analysis. Data was analysed by one-way analysis of variance (ANOVA) with Holm-Šídák's post hoc test or Student's t-test, or non-parametric equivalents, for data from mice. Data from the patient with COPD cohort was analysed by Mann-Whitney test (continuous variables) or χ^2 test (categorical variables).

Table 1 Patient characteristics								
	Placebo (n=7)		Inulin (n=9)					
	Mean	SD	Mean	SD	P value			
Age	69.71	6.50	72.78	6.46	0.18			
Gender (male, %)	42.86	N/A	66.67	N/A	0.34			
Body mass index	29.68	6.06	28.66	4.85	0.71			
Smoking pack years	56.21	20.02	49.73	24.94	0.6			
FEV1/FVC	0.48	0.09	0.48	0.13	0.95			
FEV1%	55.43	18.04	54.56	16.18	0.98			
Freq. exacerbators (n, %)	5 (71)	N/A	3 (33)	N/A	0.13			
Medications (n, %)								
Inhaled corticosteroids	5 (71)	N/A	7 (77)	N/A	0.77			
Beta agonists	7 (100)	N/A	9 (100)	N/A	>0.99			
LAMA	1 (14)	N/A	2 (22)	N/A	0.69			
Statin	2 (28)	N/A	6 (67)	N/A	0.13			
PPI	4 (57)	N/A	3 (33)	N/A	0.34			
ACE	2 (28)	N/A	2 (22)	N/A	0.77			
Beta blockers	1 (14)	N/A	1 (11)	N/A	0.85			
Angiotensin II receptor antagonist	2 (28)	N/A	1 (11)	N/A	0.37			
SSRI/SNRI	2 (28)	N/A	1 (11)	N/A	0.37			
Season during intervention (n, %)								
Spring/summer	2 (28)	N/A	3 (33)	N/A	0.84			

ACE, angiotensin-converting enzyme inhibitor; FEV1, forced expiratory volume in 1 s; FVC, forced vital capacity, LAMA, long-acting muscarinic antagonists; PPI, proton pump inhibitors; SNRI, serotonin—norepinephrine reuptake inhibitor; SSRI, selective serotonin reuptake inhibitors.

RESULTS

FMT alleviated dysbiosis and disease features in experimental COPD

To define changes in microbiome composition and the effects of FMT, C57BL/6 mice underwent microbiome normalisation to control for variability in starting microbiome composition before exposure to mainstream CS through the nose only for 12 weeks (12 wk CS), ¹²⁻¹⁵ ¹⁸⁻²⁰ with a subset of mice modelling smoking cessation with 8 weeks of CS-exposure followed by 4 weeks of rest (8 wk CS+4 wk rest). Mice were treated via passive FMT through transfer of soiled bedding from air-exposed mice to CS-exposed mice and vice versa, with controls maintained in their own bedding.

Shotgun metagenomics of faecal samples collected prior to interventions (week 0) and at completion (week 12) recovered 74 metagenome-assembled genomes (MAG)>80% complete (dereplicated at 95% identity) representing 12 families (online supplemental tables 1–4). Microbiome composition was assessed with public genomes within Genome Taxonomy Database release 06-RS202.³⁴ Metagenomic sequencing did not yield adequate sequencing coverage for further investigation of non-bacterial components, with viral signatures detected in <15% of samples and fungal signatures not identified in any samples.

All experimental groups experienced a shift in microbiome composition associated with the maturation of the mice between week 0 and 12 (from 6 to 18 weeks old), with increased α-diversity, enrichment of species belonging to the genus *Prevotella* and family *Muribaculaceae* and depletion of *Akkermansia* and

Duncaniella (a member of Muribaculaceae) species (online supplemental figure S2A-C, online supplemental table S5).

While different experimental groups had similar α-diversity at week 12, microbiome composition differed significantly (online supplemental figure S2D,E p=0.01, PERMANOVA of Bray-Curtis distances). CS-exposure was associated with increased Phocaeicola vulgatus, Muribaculaceae species Duncaniella sp001689575 and Amulumruptor sp001689515, Desulfovibrionaceae species Mailhella sp003512875 and Akkermansia muciniphila and decreased Lachnospiraceae species Muricomes sp001517425 (figure 1A,B, online supplemental tables S6, S7). CS-exposed FMT mice maintained increased abundance of most CS-associated species compared with air-exposed mice, except for the Lachnospiraceae member UBA3282 sp009774575 (MAG FTS36, online supplemental table 6). This species, along with CS-associated Mailhella sp003512875 (MAG FTS70), was identified in a multivariate analysis-derived signature distinguishing 12-week CS-exposed mice from both air-exposed and 12-week CS-exposed FMT mice (figure 1C,D, online supplemental table S8). Both species were increased with CS-exposure and decreased with FMT, consistent with a role in disease (figure 1E). Other species contributing to the FMT-associated signal were decreased with CS-exposure and increased with FMT, including obligate anaerobes Duncaniella dubosii, P. goldsteinii, Muribaculum intestinale and Mucispirillum schaedleri (figure 1D, online supplemental table S8). Similar evidence of transfer of anaerobic species to air FMT mice (online supplemental table S6) indicates that bedding swaps were an effective method of FMT, including of anaerobes.

CS-exposure induced lung inflammation characterised by increased total leucocytes, neutrophils and macrophages in bronchoalveolar lavage fluid (BALF) and immune cells in parenchyma (figure 1G,H), as well as emphysematous alveolar destruction (figure 1I,J). BALF macrophages remained elevated after smoking cessation at levels comparable to mice exposed to CS for 12 weeks, while other measures of inflammation and alveolar destruction were present but had reduced severity. Impaired lung function, with increased compliance, volume and total lung capacity, was observed after 12 weeks CS-exposure (figure 1K,M).

FMT-treated mice had significantly lower BALF and parenchymal inflammation in mice exposed to CS for 12 weeks, or with smoking cessation (figure 1E–H). Unlike smoking cessation, FMT reduced BALF macrophages and the combination of smoking cessation and FMT had additive effects by further reducing total leucocytes and parenchymal inflammation. Most importantly, FMT alleviated both emphysema and impaired lung function after CS for 12 weeks (figure 1I–M).

Thus, FMT alleviated hallmark features of COPD and improved the resolution of chronic inflammation with smoking cessation.

FMT alters systemic manifestations of COPD

Given our evidence of CS-induced systemic comorbidities,⁷ ¹² we assessed gut manifestations of COPD and systemic leucocyte populations in mice exposed to CS for 12 weeks, with and without FMT. CS-induced increases in colonic submucosal fragmentation and vascularisation, and colon tissue messenger RNA expression of the microbe-sensing pattern recognition receptors *Tlr3* and *Tlr4* was prevented by FMT, with similar trends for *Tlr2* (figure 2A–E). No significant differences were observed in expression of *Tlr9* (figure 2F).

We employed deep immune profiling using cytometry by timeof-flight with 38 immune cell markers in the bone marrow, blood and spleen. Dimensionality reduction and clustering of bone marrow cells identified 20 clusters with coherent protein expression, but few were altered (figure 3A-C). CS-exposure reduced the abundance of B cells, likely driven by a downregulation of proliferating (IdU⁺) B cells, but these effects were not alleviated by FMT (figure 3D). In blood, 25 clusters were identified (figure 3E-G). B cells were reduced by CS-exposure and partially restored by FMT (figure 3H). CS-exposure also increased blood Ly6Clo monocytes, and FMT restored their abundance to levels in air-exposed mice (figure 3H). In the spleen, 23 clusters were identified (figure 3I-K) with CD8+ conventional dendritic cells (cDCs) and B cells reduced while CD107+ progenitors and Ly6C^{lo} monocytes were increased by CS-exposure (figure 3L). FMT increased the abundance of CD8⁺ cDCs, CD107⁺ progenitors and Ly6Clo monocytes, partially restoring the CS-induced depletion of CD8a+ cDCs but enhancing the impact of CS-induced increases in CD107⁺ progenitors and Ly6C^{lo} monocytes.

Thus, FMT alleviated CS-induced colonic pathology and TLR expression, as well as CS-induced depletion of blood B cells and splenic CD8⁺ cDCs and increases in blood Ly6C^{lo} monocytes.

Correlations of lung and gut pathology with microbiota

We assessed the role of the gut microbiome in pathogenesis by fitting phenotypic data to a β-diversity ordination analysis, identifying significant associations with lymphocytes and emphysema consistent with CS-induced separation in microbiome composition (figure 4A). When smoking cessation groups were excluded to assess associations in more severe disease, total leucocytes and neutrophils were also associated with microbiome composition (figure 4B). Correlations between individual species and phenotypes identified positive correlations between Mailhella sp003512875 (FTS70) and inflammation, emphysema, colon vascularisation and Tlr4 expression (figure 4C, online supplemental table S9). Muribaculaceae species Amulumruptor sp001689515 and A. muciniphila positively correlated with lymphocytes and emphysema while A. muciniphila A correlated with lymphocytes and colon *Tlr3* expression. *M. intestinale* and Muribaculaceae species UBA7173 sp001689685 were negatively correlated with inflammation, emphysema and colon Tlr4 expression indicating a protective role.

CS-induced changes in microbiota impair responsiveness to TLR4 agonists

Given that CS-associated taxa correlated with colonic TLR expression, we assessed the effects of CS-induced dysbiosis on immune responses in vitro. RAW264.7 mouse monocytes were cultured for 24 hours in media alone, or in sterile-filtered homogenates of faeces from mice exposed to CS or air for 12 weeks. During the final 4 hours of incubation, TLR4 agonists LPS and monophosphoryl lipid A (MPLA), or the TLR2 agonist lipoteichoic acid (LTA) were added to directly stimulate TLRs. Faeces from either CS-exposed or air-exposed mice induced TNF-α production compared with media alone, but this was significantly lower with faeces from CS-exposed mice (online supplemental figure S3). LPS and MPLA induced TNF-α production at comparable levels in cells with media or faeces from air-exposed mice, but faeces from CS-exposed mice suppressed LPS-induced and MPLA-induced TNF-α. There were no significant differences in LTA-induced TNF-α production, suggesting that the impairment may be specific to TLR4.

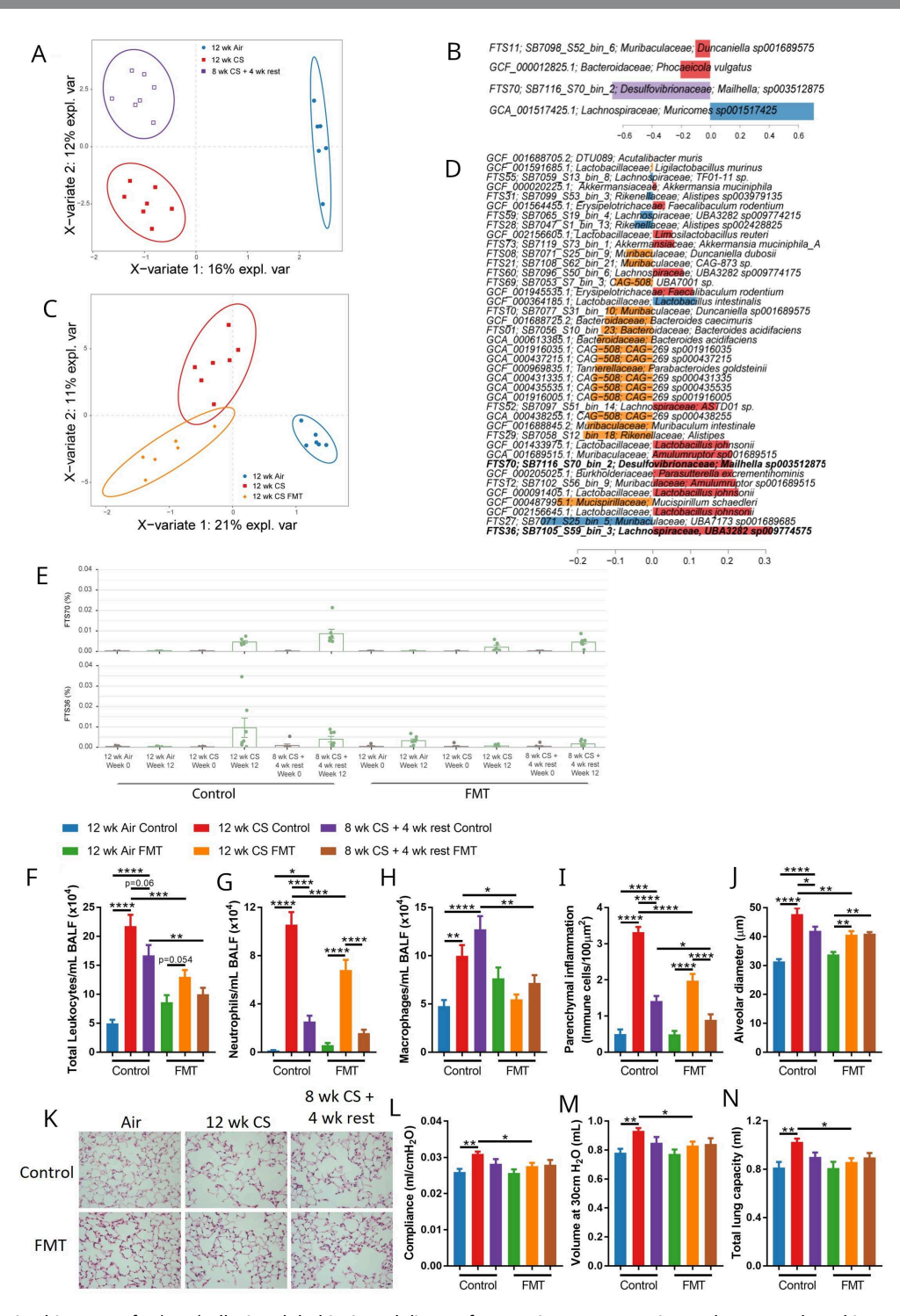


Figure 1 Faecal microbiota transfer (FMT) alleviated dysbiosis and disease features in severe experimental COPD and smoking cessation. Mice were exposed to CS or normal air for 12 weeks, or 8 weeks CS followed by 4 weeks with normal air (8 wk CS+4 wk rest). Mice also received FMT through transfer of soiled bedding or were maintained in their own bedding (Control) for 12 weeks. (A–D) Faecal samples were collected at the end of experiment (week 12) and analysed using shotgun metagenomics. (A) Multivariate analysis (sPLS-DA) of CS-exposed and air-exposed mice at week 12 demonstrating distinction between the groups along component 1 based on relative abundance at the genome level, centred log-ratio transformed and (B) species contributing to that distinction. (C) Multivariate analysis (sPLS-DA) of 12-week CS-exposed control and FMT treated mice, and air-exposed mice, demonstrating distinction between CS-exposed control and FMT mice along component 2 and (D) species contributing to that distinction. (E) Relative abundance of *Lachnospiraceae* FTS36 and *Mailhella sp003512875* FTS70 were increased with CS-exposure, which were alleviated by FMT. (F–N) Hallmark features of COPD assessed at the completion of the experiment (week 12). FMT alleviated CS-induced increases in (F–H) total leucocytes, neutrophils and macrophages in bronchoalveolar lavage fluid (BALF) and (I) parenchymal inflammation in 12-week CS and 8-week CS+4 week rest mice. FMT also alleviated CS-induced increases in (J–K) emphysema-like alveolar enlargement, and (I–N) lung function parameters of compliance, volume and total lung capacity in 12-week CS mice. N=8 per group (A–N). Data presented as mean±SEM. *=p<0.05; **=p<0.01; ***=p<0.001; ****=p<0.001; ****=p<0.0001 using one-way analysis of variance with Holm-Sidak's post hoc analysis (F–N). COPD, chronic obstructive pulmonary disease; CS, cigarette smoke; sPLS-DA, sparse Partial Least-Squares Discriminant Analysis.

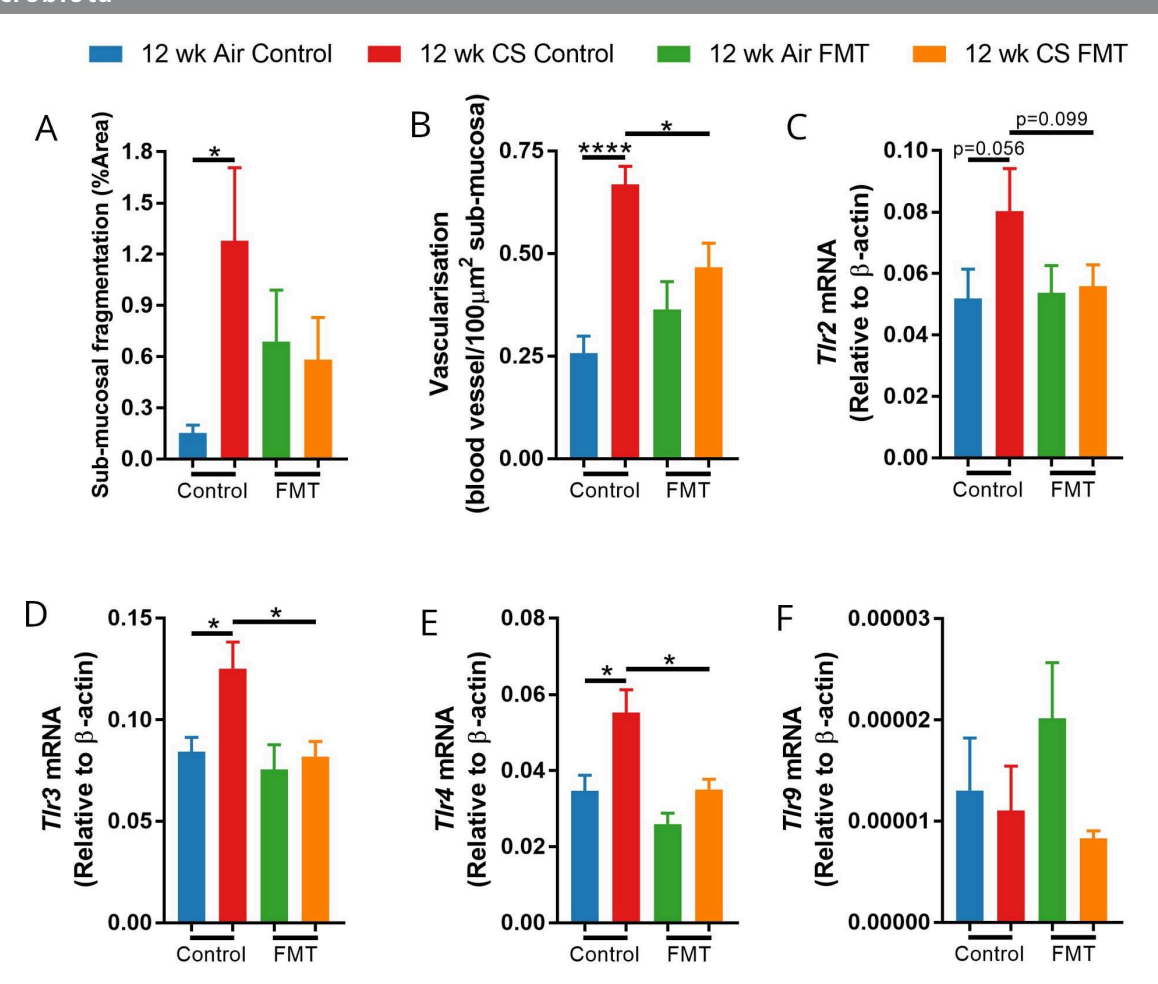


Figure 2 Faecal microbial transfer (FMT) alleviated cigarette smoke (CS)-induced colon histopathology and microbial sensor expression changes. (A–F) Mice were exposed to CS or normal air for 12 weeks, and received FMT through transfer of soiled bedding or were maintained in their own bedding (Control). FMT alleviated CS-induced increases in (A) submucosal fragmentation, (B) vascularisation and expression of (C) *Tlr2* (non-significant), (D) *Tlr3* and (E) *Tlr4* in colon tissue. (F) Expression of *Tlr9* was not altered by either CS or FMT. N=7–8 per group. Data presented as mean±SEM. *=p<0.05 using one-way analysis of variance with Holm-Sidak's post hoc analysis. mRNA, messenger RNA.

CS-associated microbiota reduce colon innate immune cells but promote lung inflammation

Chronic CS exposure induces gastrointestinal inflammation, and the suppression of TLR4 and other innate responses by CS-associated microbiota may provide a competitive advantage in this environment. To further explore the impact of CS-associated microbiota on innate immunity *in vivo*, mice received antibiotics in drinking water for 7 days to deplete microbial communities. After antibiotics were removed, microbial communities were allowed to recover naturally or were recolonised through oral gavage of faecal homogenates from air or CS-exposed mice. Donors for FMT were mice from separate experiments, and experimental mice in this model received no direct CS exposure. Innate immune cell profiles in the colon and lung were assessed by flow cytometry after 10 days.

There were no changes in innate immune populations when antibiotic-depleted microbiota were recovered naturally or were recolonised with microbiota from air-exposed mice (figure 5A–G; online supplemental figure S4). However, recolonisation with faeces from CS-exposed mice reduced the number of colonic monocytes, immature macrophages (Ly6C+major histocompatibility complex (MHC)-II+) and mature macrophages (Ly6C-MHC-II+), including reduced slow-turnover (T-cell immunoglobulin and mucin domain containing (TIM)4-CD4+) and long-lived, self-renewing tissue resident

macrophages (TIM4+CD4+; figure 5A-E). Similarly, colonic neutrophils and eosinophils were also depleted in these mice (figure 5F,G). To identify the impact of gut microbiota on the gut-lung axis in the absence of direct CS exposure, lung granulocyte populations were also assessed. Recolonisation with faeces from CS-exposed mice promoted lung inflammation, increasing interstitial macrophages and eosinophils (figure 5H,I; online supplemental figure S5).

Thus, microbiota from CS-exposed mice directly exerts differing effects across the gut-lung axis, with suppressed innate immune responses in the colon but induction of macrophage-driven and eosinophil-driven inflammation in the lungs, even in the absence of CS exposure.

Mutual exclusion contributes to the protective effects of FMT

FMT reduced the abundance of *Lachnospiraceae* member *UBA3282 sp009774575* and *Mailhella sp003512875* in CS-exposed mice (figure 1C,D, online supplemental table S8). While FMT-mediated modification of local and systemic immune responses may suppress pathogenic taxa, competition from bacteria introduced through FMT may also contribute to protective effects. To assess the role of competitive inhibition, we identified non-random patterns of co-occurrence in our metagenomics data set using the CoNET Cytoscape application.²⁸

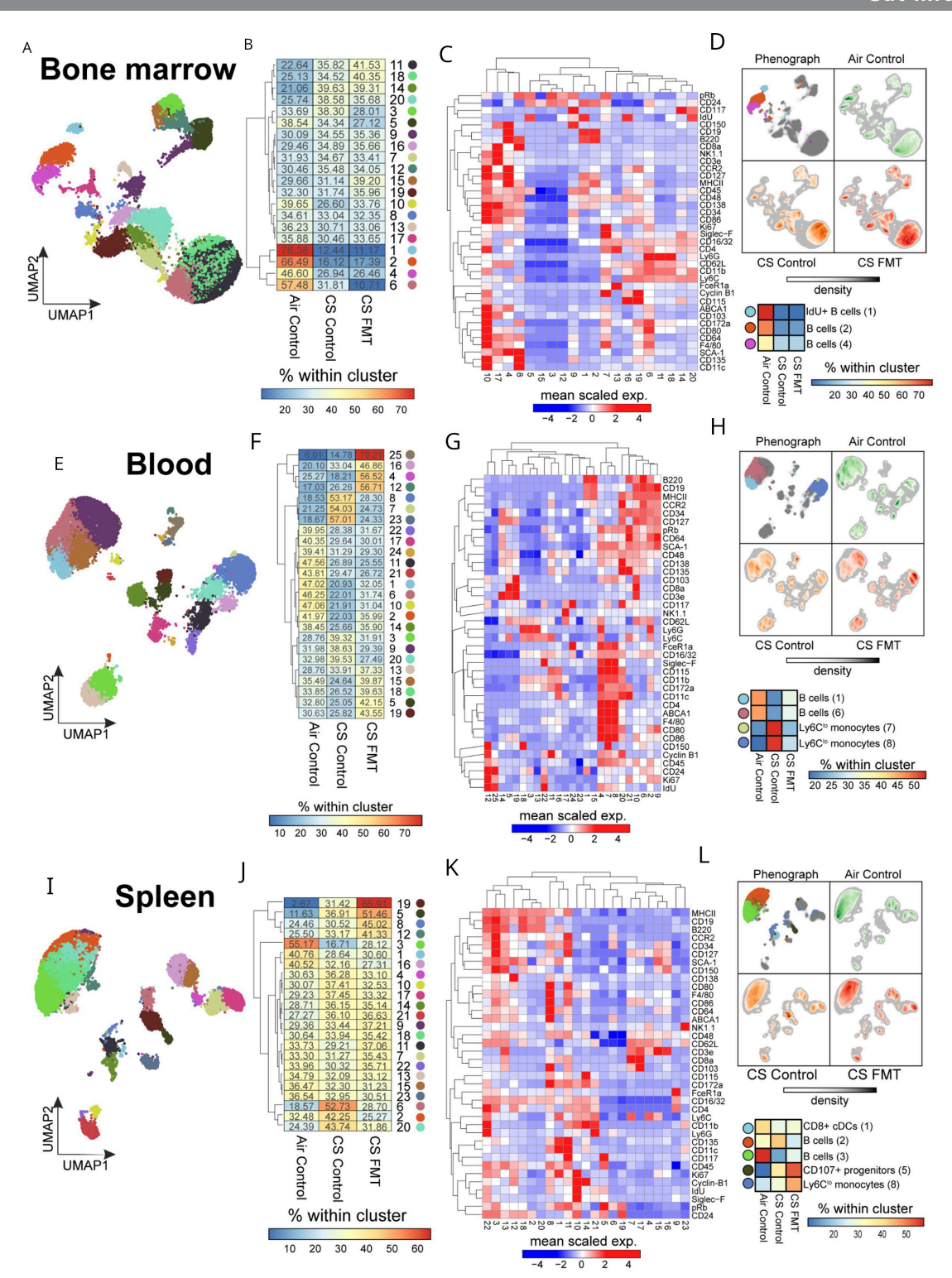


Figure 3 Cigarette smoke (CS)-exposure altered systemic leucocyte populations, and faecal microbial transfer (FMT) alleviated depletion of some blood and splenic populations. (A-I) Mice were exposed to CS or normal air for 12 weeks and received FMT through transfer of soiled bedding or were maintained in their own bedding (Control). Cell abundances were quantified using cytometry by time-of-flight. (A,B) Dimensionality reduction and clustering of bone marrow cells identified 20 clusters of cells (C) based on the scaled mean marker expression. (D) Uniform Manifold Approximation and Projection (UMAP) and a confusion matrix of the normalised frequencies of clusters demonstrated CS-induced depletion of B cells and iododeoxyuridine⁺ B cells which was not alleviated by FMT. (E,F) Dimensionality reduction and clustering of blood cells identified 20 clusters of cells (G) based on the scaled mean marker expression. (H) UMAP and a confusion matrix of the normalised frequencies of clusters demonstrated a CS-induced depletion of B cells and increase of Ly6C^{lo} monocytes, which were alleviated by FMT. (I,J) Dimensionality reduction and clustering of splenic cells identified 23 clusters of cells (K) based on the scaled mean marker expression. (L) UMAP and a confusion matrix of the normalised frequencies of clusters demonstrated CS-induced depletion of CD8⁺ conventional dendritic cells (cDCs) and B cells, and a CS-induced increase of CD107⁺ progenitors and Ly6C^{lo} monocytes. FMT increased the abundance of CD8⁺ cDCs, CD107⁺ progenitors and Ly6C^{lo} monocytes compared with CS control mice, partially reducing CD8⁺ cDCs but enhancing the CS-induced increases in CD107⁺ progenitors and Ly6C^{lo} monocytes. N=6 per group.

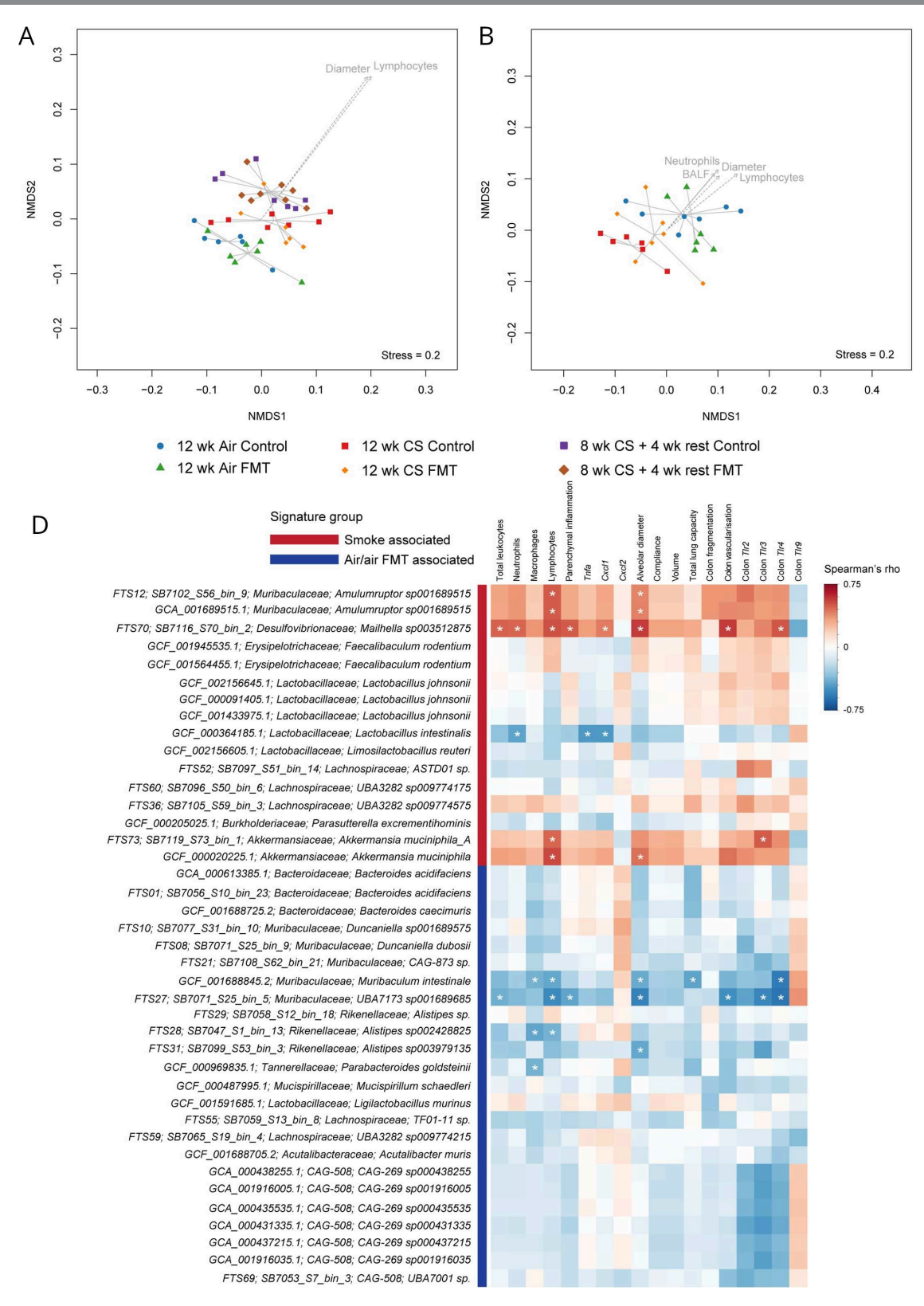


Figure 4 Cigarette smoke (CS)-associated bacterial species positively correlate with phenotypic measurements. (A–C) Mice were exposed to CS (12 wk CS) or normal air (Air) for 12 weeks, or 8 weeks CS followed by 4 weeks with normal air (8 wk CS+4wk rest). Mice also received faecal microbiota transfer (FMT) of soiled bedding or were maintained in their own bedding (Control). (A, B) Non-metric multidimensional scaling (NMDS) ordination plot of Bray-Curtis distances with phenotypic variables significantly associated with CS and/or FMT fitted to axes. Lung compliance was excluded due to colinearity with volume. (A) Lymphocytes and alveolar diameter were significantly associated with microbiome composition (Benjamini-Hochberg, p<0.05). (B) A similar analysis was performed excluding smoking cessation mice (8 wk+4 wk rest), which also identified total leucocytes in bronchoalveolar lavage (BALF) and neutrophils. (C) Spearman's correlation between phenotypic data and relative abundance of genomes separating CS-exposed mice (red bar) from air-exposed mice or CS-exposed mice receiving FMT (blue bar). Squares marked with an internal asterisk have p<0.05, demonstrating key associations with bacteria. N=8 per group.

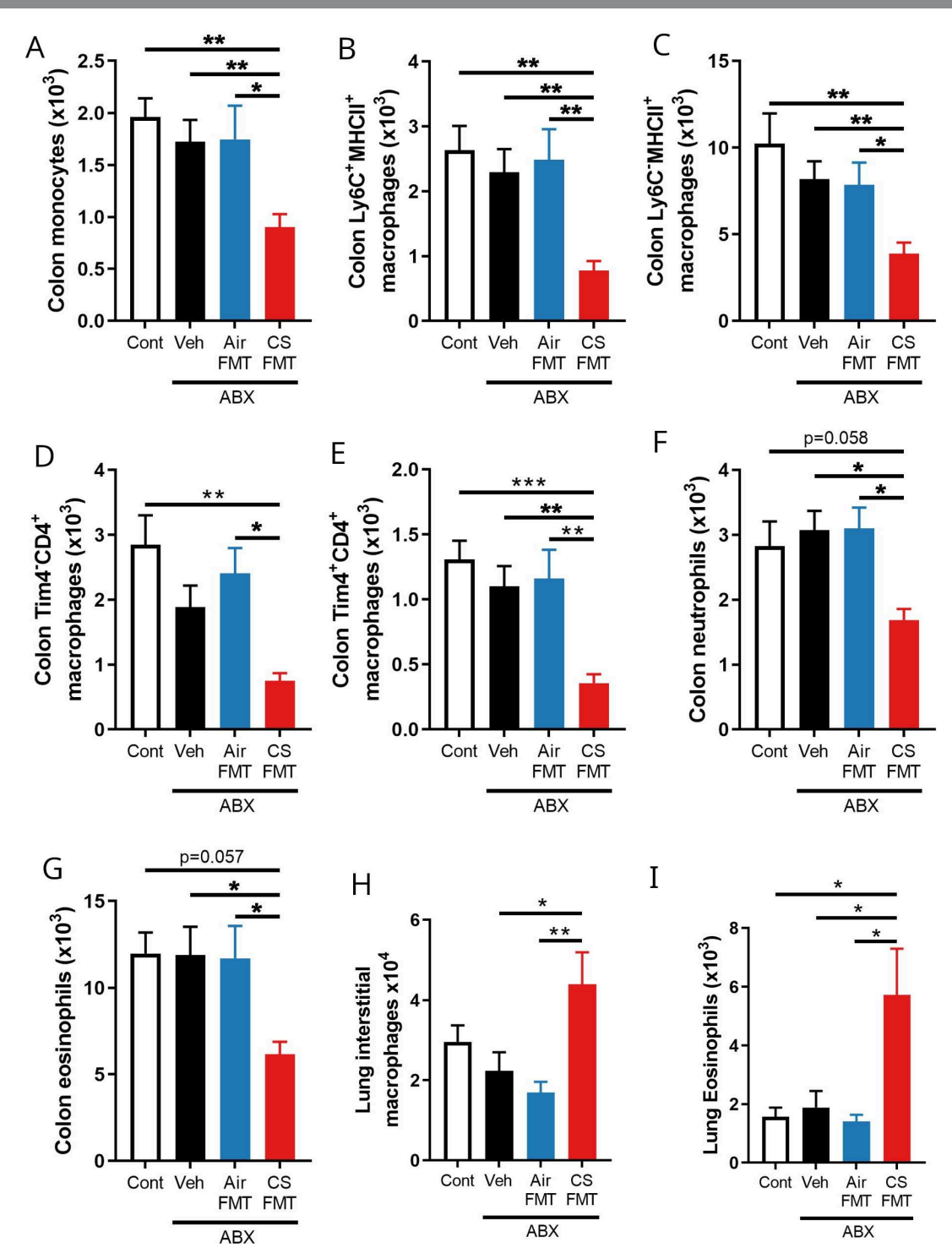


Figure 5 Innate immune cells are reduced in the colon but increased in the lungs after colonisation with microbiota from CS-exposed mice. Microbiota were depleted by antibiotics (ABX) for 7 days before mice were recolonised with faeces from separate air-exposed (Air FMT) or CS-exposed donors (CS FMT) for 10 days. A subset of mice received vehicle (Veh, phosphate-buffered saline+0.05% L-cysteine) to model natural recolonisation. Innate immune cells in the colon and lung were enumerated by flow cytometry. Colon (A) monocytes, (B) immature macrophages and (C) mature macrophages were reduced by CS FMT, including reduction (D) in slow turnover and (E) long-lived, tissue resident macrophages. (F) Colonic neutrophils and (G) eosinophils were also reduced by CS FMT. CS FMT increased (H) lung interstitial macrophages and (I) eosinophils. N=9-11 per group. Data presented as mean±SEM. *=p<0.05; **=p<0.01; ***=p<0.001; using one-way analysis of variance with Holm-Sidak's post hoc analysis. CS, cigarette smoke; FMT, faecal microbial transfer; MHC, major histocompatibility complex.

Of the 424 relationships identified, there were 308 co-presence and 116 mutual exclusion relationships (figure 6; online supplemental table S10). Most CS-associated taxa, including *P. vulgatus*, *Duncaniella sp001689575*, *Amulumruptor sp001689515*, *Mailhella sp003512875* and *A. muciniphila* displayed co-present

relationships with other CS-associated taxa but no evidence of mutual exclusion with air-associated or FMT-associated taxa. Additionally, *Lachnospiraceae* member *UBA3282 sp009774575* and air-associated *Muricomes sp001517425* were not identified in any co-present or mutually exclusive relationships. However,

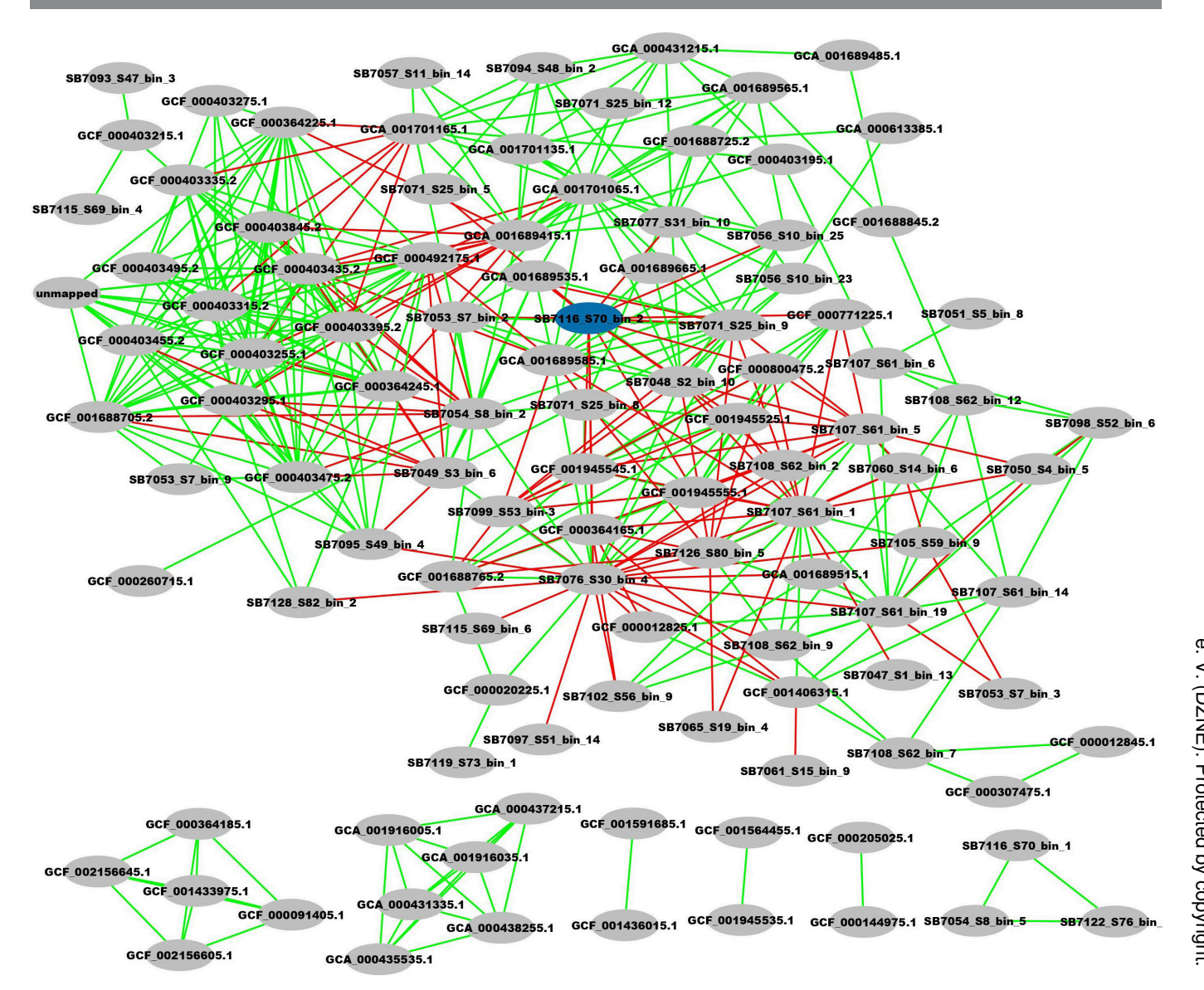


Figure 6 *Mailhella sp003512875* (blue ellipse; SB7116_S70_bin_2) has patterns of mutual exclusion with air/FMT-associated taxa. Mice were exposed to CS or normal air for 12 weeks, or 8 weeks CS followed by 4 weeks with normal air (8 wk CS+4 wk rest). Mice also received FMT through transfer of soiled bedding or were maintained in their own bedding (Control) for 12 weeks. Faecal samples were collected at the end of experiment (week 12) analysed using shotgun metagenomics, and non-random patterns of co-occurrence identified using the CoNET Cytoscape application. Patterns of co-occurrence (308, green lines) were more abundant than patterns of mutual exclusion (116, red lines). CS-associated taxa *Phocaeicola vulgatus*, *Duncaniella sp001689575*, *Amulumruptor sp001689515*, *Mailhella sp003512875* and *Akkermansia muciniphila* displayed co-present relationships with other CS-associated taxa but no evidence of mutual exclusion with air-associated or FMT-associated taxa. *Lachnospiraceae* member *UBA3282 sp009774575* was not identified in any patterns of co-present or mutually exclusive relationships. However, *Mailhella sp003512875* had 15 non-random patterns indicating mutual exclusion, including with Air/FMT-associated taxa *Duncaniella sp001689575*, *Duncaniella dubosii* and *UBA7173 sp001689685*. N=48 (eight samples per group from six experimental groups).

15 non-random patterns indicating mutual exclusion (13% of all mutual exclusions observed) were identified with *Mailhella sp003512875*, including with Air/FMT-associated taxa *Duncaniella sp001689575*, *D. dubosii* and *UBA7173 sp001689685*. Thus, while not explaining all protective effects, FMT introduced taxa with which mutual exclusion relationships to *Mailhella sp003512875* were observed.

CS-associated taxa are not introduced during smoking

Bacteria have been identified in CS by both culture-dependent and independent methodologies.³⁵ ³⁶ To determine whether CS-associated taxa were introduced to mice directly during CS-exposure, smoke from a 3R4F research cigarette was bubbled

through sterile phosphate-buffered saline (PBS). This process was repeated independently with four different cigarettes and independent negative controls. Aliquots were subjected to DNA extraction and analysis by 16S rRNA gene sequencing. After quality filtering and adapter trimming, reads from both CS extract (CSE) and PBS samples were exceptionally low (115.8±20.22 reads vs 329.8±503.6 reads). A total of 55 amplicon sequencing variants (ASVs) were identified, none of which were present in >1 CSE sample while absent from PBS. Due to the low biomass, ASVs were collapsed to genera/family level and relative abundances were broadly similar between CSE and PBS samples, although there was significant inter-sample variability (online supplemental figure S6A,B). Notably, there was no

evidence that CS-associated taxa (eg, *Duncaniella sp001689575* and *Amulumruptor sp001689515*, *Mailhella sp003512875*, *A. muciniphila* and *UBA3282 sp009774575*) were enriched in CSE samples. CSE were also cultured on Yeast Casitone Fatty Acids agar under anaerobic conditions, ³⁷ but no colonies were observed after 48 hours.

Experimental COPD and FMT were consistently associated with bacterial taxa

To validate our findings and explore temporal changes in the microbiome up until disease onset, mice were exposed to CS for 8 weeks with passive FMT through transfer of soiled bedding. Changes in gut microbiota were profiled weekly using 16S rRNA gene sequencing of fresh faecal samples collected directly from each mouse for the duration of the experiment (online supplemental tables 11-12). Microbiota composition in different groups were distinguishable from week 1 and continued to transition over time (online supplemental figure S7A-C). Multivariate analysis using sPLS-DA revealed CS-associated separation at week 8 (online supplemental figure S7D) driven primarily by five ASVs, including two Muribaculaceae family members which increased in CS-exposed mice (without FMT) from week 3 but only increased in CS-exposed mice receiving FMT after 6 weeks and decreased in subsequent weeks (online supplemental figure S7E,F).

We also explored microbiome changes in gastrointestinal tissues collected at week 8 and observed similar CS-associated separation in colons, driven by the previously identified *Muribaculaceae* ASVs plus *Desulfovibrionaceae* and *Lachnospiraceae* species (online supplemental figure S8A,D). CS-associated separation was less clear in the caecum (online supplemental figure S8B,E) and was not evident in the ileum (online supplemental figure S8C,F). However, ileum samples did reveal separation between CS-exposed FMT and CS-exposed control mice, with the abundance of distinguishing ASVs in the FMT group resembling air-exposed levels (online supplemental figure S8G-K).

Phenotypic measures were collected at the end of the experiment (week 8), with CS-induced induced inflammation, alveolar destruction and lung function impairment (online supplemental figure S7G-P). FMT blunted the CS-induced increase in BALF cells and completely suppressed changes in total lung capacity (online supplemental figure S7G-I,P). Similar phenotypic changes were observed with active FMT administered by oral gavage, confirming the involvement of gut microbiota (online supplemental figure S9A-F).

Relative abundance of CS-associated *Muribaculaceae 91ca* in faeces at the final time point (week 8) positively correlated with total leucocytes, emphysema and work of breathing (online supplemental figure S10A; online supplemental table S13). ASVs associated with non-smoking had a variable abundance pattern across the experiment and did not correlate with any phenotypic scores (online supplemental figure S10B-D).

Thus CS-induced experimental COPD is reproducibly associated with changes in gut microbiota, particularly a *Muribaculaceae* family member and FMT alleviated hallmark features of disease.

Multiomics implicate downregulation of microbial glucose and starch metabolism in experimental COPD

To assess changes in microbial function, we characterised the faecal proteome (online supplemental table S14) and integrated the results with bacterial abundances. Correlations with individual MAGs did not reveal clear associations, but genera

CAG-307, Staphylococcus, Bilophila, Aerococcus, CAG-411, Corynebacterium, Rikenella, Lactonifactor, Acetivibrio and Absiella were most frequently correlated with the microbial proteome (R≥0.7; p<0.05; figure 7A, online supplemental table S15).

Of these proteins correlated with bacterial genera, 12 were significantly altered in at least one experimental group (online supplemental table S16). Chaperone protein AELOFPMA_23737 and urease subunit alpha GFDOOBDM_36378 were increased by 12 weeks CS-exposure, but not in smoking cessation and were not alleviated by FMT (figure 7B,C).

Four proteins were altered by both CS-exposure and FMT (figure 7D-G). Alkyl hydroperoxide reductase subunit C GDJJNAEL_42303, an antioxidant protein, was increased after 12 weeks of CS-exposure and alleviated by smoking cessation and FMT (p=0.052) (figure 7D). Rubrerythrin BGMILIAL 35735, also implicated in oxidative stress responses, had a reverse pattern and was decreased after 12 weeks of CS-exposure and after smoking cessation and increased by FMT (figure 7E). Phosphoglycerate kinase AAEHAFLO 09769 and malate dehydrogenase EAAGGHIE 49748, implicated in glucose metabolism and energy generation, were both increased by 12 weeks of CS-exposure and, to a lesser extent, after smoking cessation (figure 7F,G). While FMT alleviated the CS-induced increase in AAEHAFLO 09769, it further increased EAAGGHIE 49748.

Metabolite profiling in the caecum contents of a separate cohort of CS-exposed mice identified reduced abundance of microbiota-derived amino acid metabolites including tryptophan-derivatives indolelactate, indole-3-carboxylic acid, indoleacetate and indolepropionate, phenylalanine derivative phenyllactate and isoleucine-derivative 2-hydroxy-3-methylvalerate (online supplemental figure S11A-F). Isovalerate, produced by microbial fermentation of leucine, was increased (online supplemental figure S11G). Host-derived primary bile acids were not altered by CS (online supplemental figure S12A-E) but secondary bile acids, produced from primary bile acids by microbial biotransformation, were significantly elevated (online supplemental figure S8F-K). Moreover, glycolysis, gluconeogenesis, starch and sucrose metabolism components were downregulated (figure 7H-L) which, while not specific for microbiota, were consistent with changes observed in faecal proteomics. Thus, metabolomics and proteomics implicated a downregulation of glucose and starch metabolism in CS-exposed mice, which was altered by FMT.

Dietary resistant starch alleviated inflammation and emphysema in experimental COPD

Given the changes in microbial glucose and starch metabolism, we assessed whether dietary supplementation with complex carbohydrates improved disease outcomes. Mice were exposed to CS (8 weeks), and fed either control diet or an equivalent diet with all carbohydrates as resistant starch (high amylose maize starch) which is not digested by the host, increasing the availability to microbiota. Resistant starch alleviated CS-induced airway inflammation and prevented CS-induced increases in alveolar diameter (figure 8A–E), consistent with the protective effects of FMT.

At the experimental endpoint, faecal microbiota were profiled using 16S rRNA gene sequencing. Resistant starch reduced α -diversity in both air-exposed and CS-exposed

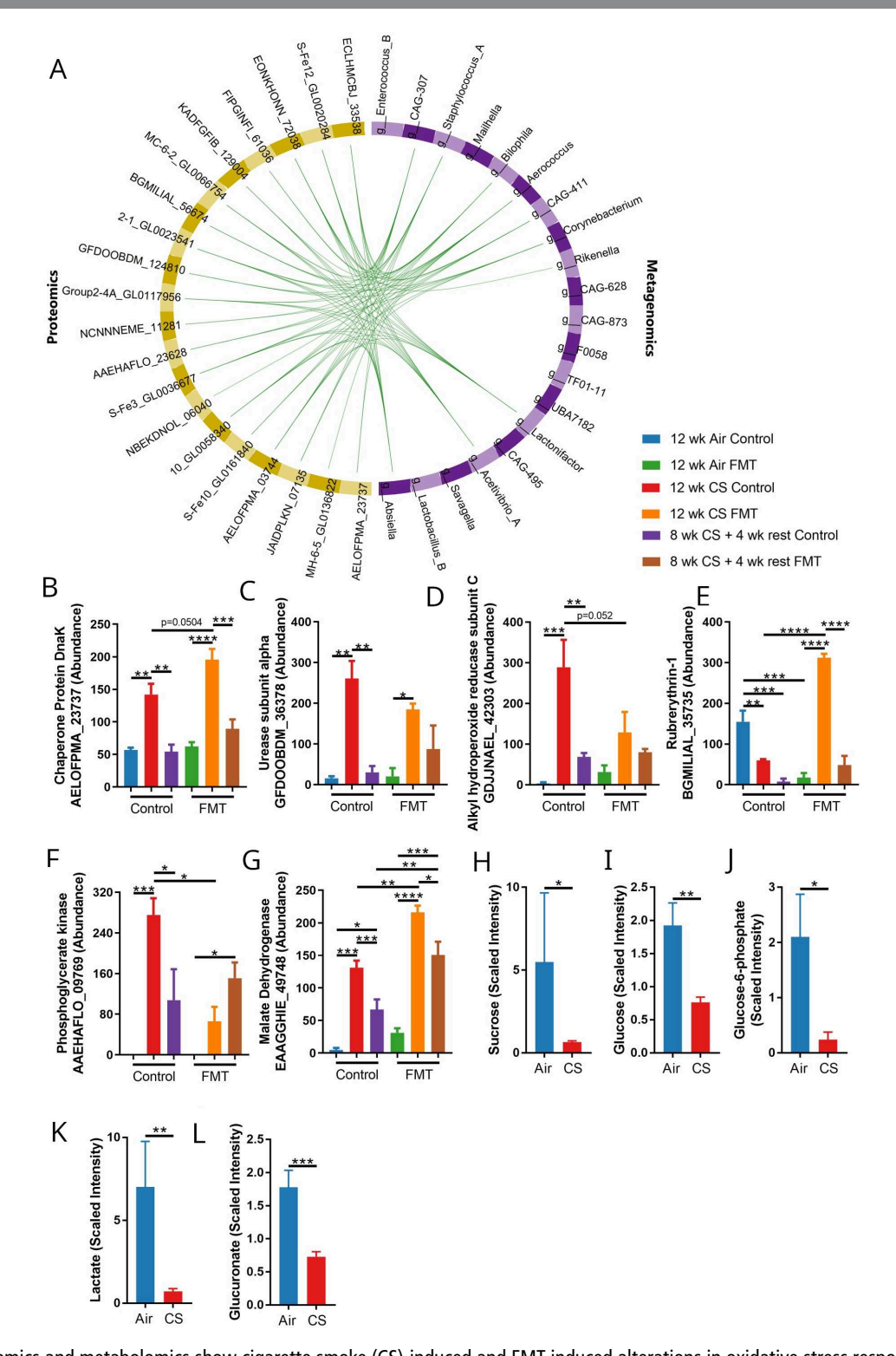


Figure 7 Proteomics and metabolomics show cigarette smoke (CS)-induced and FMT-induced alterations in oxidative stress responses and glucose metabolism. (A—H) Mice were exposed to CS (12 wk CS) or normal air (Air) for 12 weeks, or 8 weeks CS followed by 4 weeks with normal air (8 wk+4 wk rest). Mice also received FMT through transfer of soiled bedding or were maintained in their own bedding (Control) for 12 weeks. (A) Pearson correlation of highly abundant bacterial genera (purple) from metagenomics and proteins (yellow) from proteomics using the MixOmics DIABLO package (green lines; correlation coefficient=0.7, Bonferroni-adjusted p<0.05). (B) Abundance of chaperone protein AELOFPMA_23737 and (C) urease subunit alpha GFDOOBDM_36378 were increased by 12 weeks CS-exposure. (D) Abundance of oxidative stress-responsive proteins GDJJNAEL_42303 and (E) BGMILIAL_35735 demonstrated increases and decreases after CS-exposure, respectively, which was alleviated by FMT. (F) Abundance of energy metabolism proteins AAEHFLO_09769 and (G) EAAGGHIE_49748 were increased by CS-exposure, which was alleviated and enhanced by FMT, respectively. (H—I) Mice were exposed to CS or air for 12 weeks, and metabolites in caecum contents assessed. Components of the glycolysis and gluconeogenesis, or starch and sucrose metabolism pathways were downregulated in CS-exposed mice. N=3 (A—G) or 8 per group (H—I). Data presented as mean±SEM. *=p<0.05; **=p<0.01; ****=p<0.001; ****=p<0.0001 using one-way analysis of variance with Holm-Sidak's post hoc analysis (C—G) or unpaired Student's t-test on log-transformed data (H—I). FMT, faecal microbial transfer.

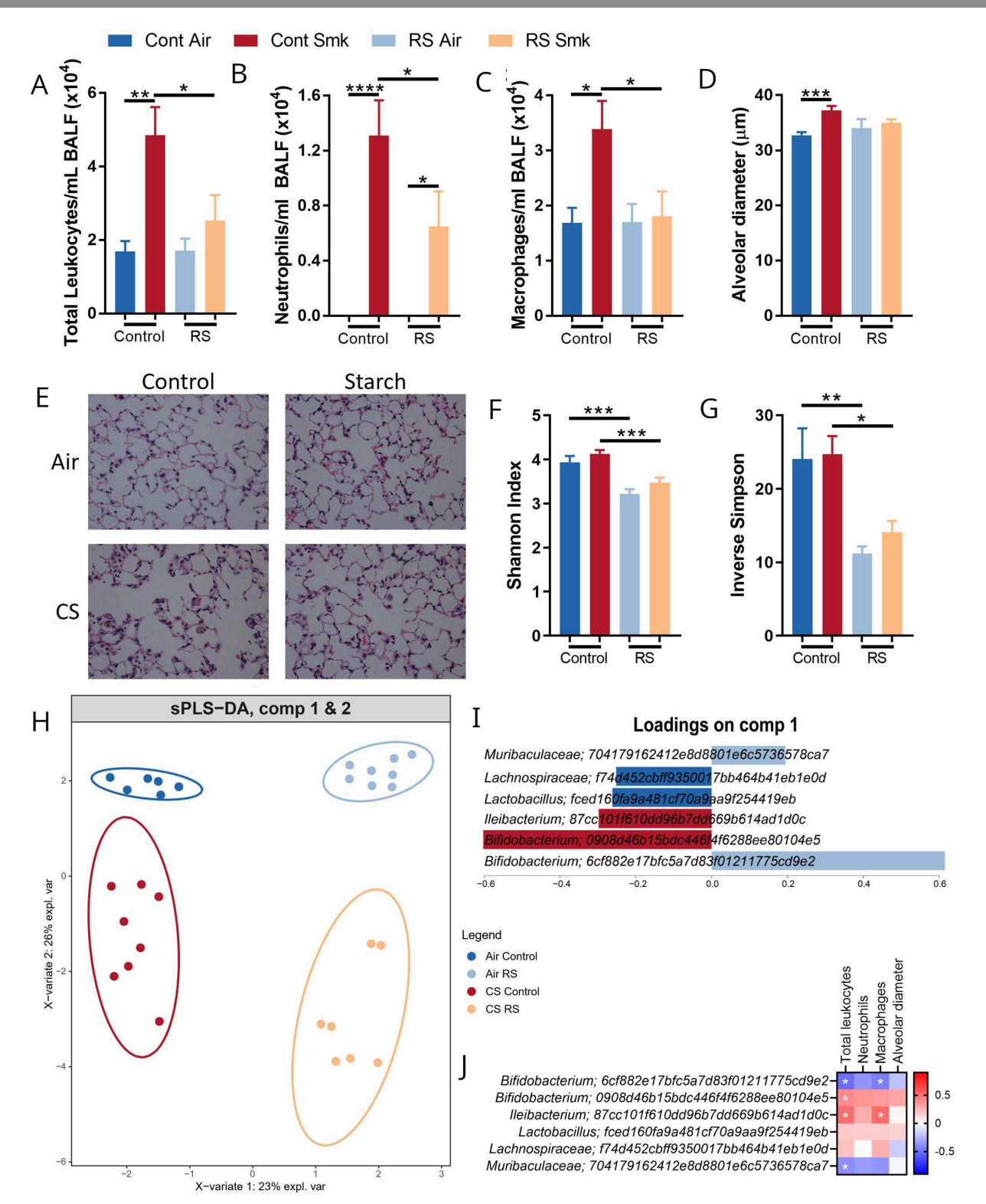


Figure 8 High resistant starch intake alleviated cigarette smoke (CS)-induced inflammation and emphysema. (A–D) Mice were exposed to CS or normal air for 8 weeks. Beginning 2 weeks prior to exposure, mice were fed a control or resistant starch (RS) diet. RS diet alleviated CS-induced increases in (A) total leucocytes, (B) neutrophils and (C) macrophages in bronchoalveolar lavage fluid (BALF) and prevented (D, E) CS-induced alveolar destruction. (E–J) Faecal microbiome was characterised by 16S rRNA gene sequencing. RS reduced α-diversity measure by (F) Shannon and (G) inverse Simpson index. (H) Multivariate analysis (sPLS-DA) indicated RS-induced and CS-induced separation of microbiome samples using PERMANOVA of Bray-Curtis distances, driven largely by (I) altered *Bifidobacterium* amplicon sequencing variants (ASVs). (J) ASVs contributing to separation were correlated with inflammation in BALF. N=6–14 per group. Data presented as mean±SEM. *=p<0.05; **=p<0.01; ***=p<0.001; ****=p<0.0001 using (A–G) one-way analysis of variance with Holm-Sidak's post hoc analysis or (J) Spearman's correlation. sPLS-DA, sparse Partial Least-Squares Discriminant Analysis.

COPD, chronic obstructive pulmonary disease.

in BALF.

Table 2 Exacerbation frequency, COPD Assessment Test (CATest) and St Georges Respiratory Questionnaire symptom scores (SGRQ) in patients with COPD receiving 4 weeks placebo (N=7) or inulin (N=9) supplement

	Placebo		Inulin		
	Mean	SD	Mean	SD	P value
Number of exacerbations	4 (57%)	N/A	1 (11%)	N/A	*0.048
Pretreatment CATest score	14.33	1.16	17.13	7.18	>0.99
Post-treatment CATest score	16.00	1.00	12.88	5.33	>0.99
Δ CATest score	1.67	2.08	-4.25	2.49	*0.01
Pretreatment SGRQ score	40.49	13.08	42.52	16.94	>0.99
Post-treatment SGRQ score	41.91	3.24	36.17	14.51	>0.99
Δ SGRQ total score	1.43	9.94	-6.34	6.07	0.27
*p < 0.05.					

mice (figure 8F,G), and multivariate analysis using sPLS-DA demonstrated clear separation between all experimental groups (figure 8H; p=0.01, PERMANOVA of Bray-Curtis distances). This was driven primarily by a shift in *Bifidobacterium* ASVs, one increased by resistant starch and one decreased (figure 8I). Multiple ASVs correlated with disease features (figure 8J; online supplemental table S17) including the resistant starch-associated *Bifidobacterium* which was negatively correlated with total leucocytes and macrophages

Inulin supplementation reduced symptoms and exacerbations in human COPD

To explore whether these findings translated into humans, we performed a small, preliminary pilot study with a randomised, double-blind, placebo-controlled study in patients with COPD receiving supplements of inulin, a common fermentable fibre, for 4 weeks. There were no differences between placebo-treated (N=7)and inulin-treated (N=9) patients in age, gender, BMI, smoking history, lung function, proportion of frequent exacerbators (≥2 exacerbations in 12 months), medication use or seasonality of intervention (table 1). Oral inulin resulted in fewer self-reported exacerbations (worsening or respiratory symptoms requiring additional pharmaceutical intervention) during the intervention period (1/9 patients, 11%) than placebo (4/7 patients, 57%) (table 2) and improved health-related quality of life measured by two validated instruments; the COPD Assessment Test (CATest) and the St Georges Respiratory Questionnaire (SGRQ). Both CATest and SGRQ scores were lower (improved symptoms) after inulin treatment than at baseline, exceeding the Minimally Important Clinical Difference.³⁹ There was no reduction in either score after placebo (table 2), but only the change in CATest score was significantly different in inulin-treated patients compared with placebo.

Faecal microbiota composition before and after receiving inulin was assessed by 16S rRNA gene sequencing. Although no differences in α -diversity were observed (figure 9A,B), microbiome composition differed significantly after inulin consumption, primarily driven by increased abundance of *Bacteroides* (figure 9C,D p=0.01, PERMANOVA of Bray-Curtis distances).

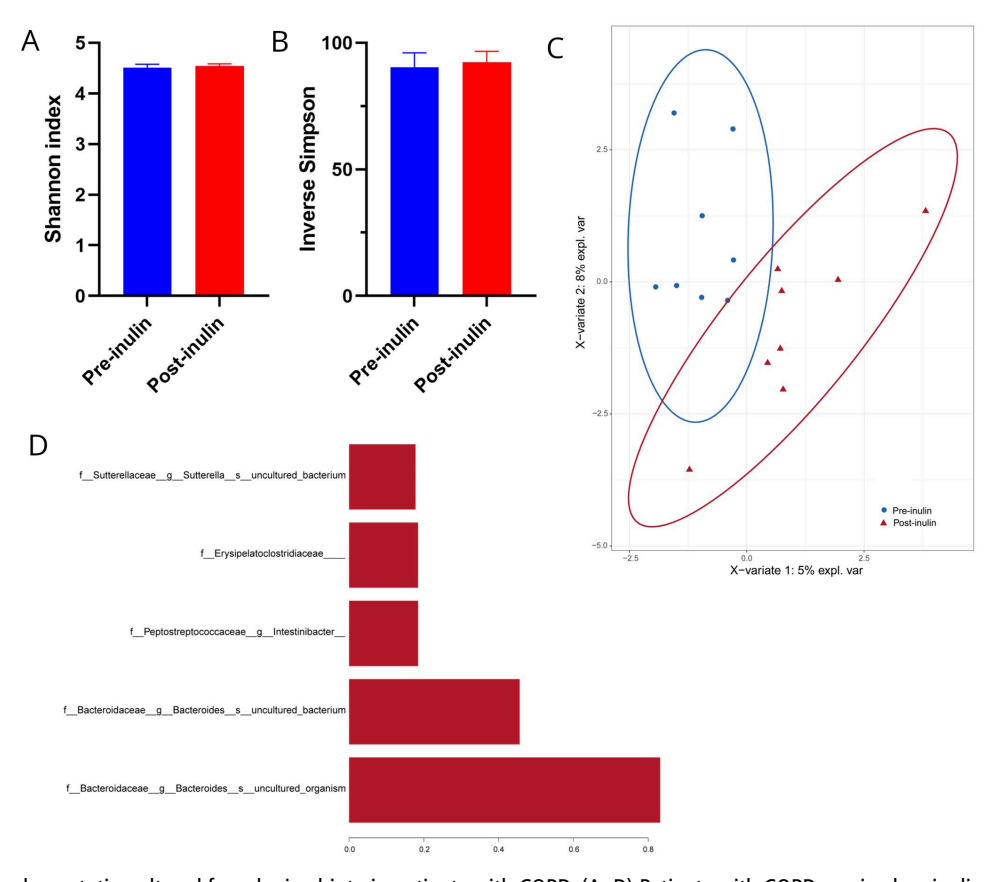


Figure 9 Inulin supplementation altered faecal microbiota in patients with COPD. (A—D) Patients with COPD received an inulin supplement for 28 days. Faecal microbiome composition was assessed before (pre-inulin) and after (post-inulin) inulin supplementation by 16S rRNA amplicon sequencing. (A—B) Shannon and Simpson diversity indices were not altered by inulin supplementation. (C) Multivariate analysis (sparse Partial Least-Squares Discriminant Analysis) demonstrating distinction between pre-inulin and post-inulin samples using PERMANOVA of Bray-Curtis distances and (D) species contributing to that distinction. COPD, chronic obstructive pulmonary disease.

DISCUSSION

CS-induced changes were broadly similar across several experiments, with Muribaculaceae Desulfovibrionaceae and Lachnospiraceae members increased after 8 and 12 weeks and correlating with disease phenotypes. FMT only partially alleviated CS-induced changes in microbiome composition, likely due to continued selective pressure with continuous smoke exposure or incomplete microbiota replacement using the bedding swap FMT. Bedding swaps, while not the most controlled method of FMT, 40 were used in most experiments as repeated oral gavage affects histopathology and lung function in mice. 41 Nevertheless, FMT reproducibly alleviated inflammation, emphysema, impaired lung function and gastrointestinal pathology and analysis of mice receiving FMT demonstrated effective transfer of bacteria, including obligate anaerobes such as D. dubosii, P. goldsteinii, M. intestinale and M. schaedleri. Further, our initial findings were validated by FMT using oral gavage in a smoking model, and transfer of faeces from smoking mice into naïve mice after antibiotic-induced microbiome depletion increased lung inflammation, confirming that gut microbiota have substantial effects on disease. Minor differences in microbiome changes between studies were expected due to natural variability, 42 and cage/batch effects were controlled by microbiome normalisation. Together, these findings demonstrate effective alleviation of disease by FMT and associations with bacterial taxa across multiple independent experiments.

Reproducibility between experimental models of COPD has proven challenging, 10 11 as has the correspondence between changes observed in murine models and samples from human patients with COPD. Australian patients with COPD had reduced abundance of Desulfovibrionaceae member Desulfovibrio piger in faeces, but increased Lachnospiraceae species, including Sellimonas intestinalis, that negatively correlated with lung function.8 Chinese mild COPD cohorts had higher abundance of Prevotellaceae while patients with severe disease had lower abundance of Bacteroidaceae and Fusobacteriaceae, 43 and identified that Bacteroides sp CAG875, Christensenella minuta and Clostridium sp Marseille-P2538 were the most abundant species in faeces differentiating healthy donors from patients with COPD. 44 In a Korean cohort, patients with COPD were differentiated from asymptomatic smokers by 17 bacterial groups including lower Prevotella copri, Dialister succinatiphilus and Catenibacterium mitsuokai and increased Bacteroides fragilis and Bifidobacterium longum, 45 highlighting the challenges of identifying a consistent microbial marker of disease especially given the demographic differences between cohorts. Some studies in mice have identified that CS-exposure increased *Lachnospiraceae* abundance, ¹¹ while others report decreases. 10 Our new data agrees with that from our previously published Australian cohort and other animal models, identifying a role for *Lachnospiraceae* in disease, but is the first study to implicate Muribaculaceae species in patients with COPD or animal models. Although more predominant in the murine microbiome, this family is present in humans and may have roles in disease.8 Two Muribaculaceae species, M. intestinale and UBA7173 sp001689685, negatively correlated with inflammation and emphysema, highlighting the importance of assessing the microbiome at higher taxonomic resolution. 10

The precise causes of dysbiosis in COPD have not been defined. Several bacteria have been identified in CS by both sequencing and culture-based techniques, including *Acinetobacter*, *Bacillus*, *Burkholderia*, *Clostridium*, *Klebsiella*, *Pseudomonas*, *Serratia*, *Campylobacter*, *Enterococcus*, *Proteus*, *Staphylococcus* and *Pantoea* species.^{35 36} However, none of these taxa contribute to

the CS-associated microbiome in our model, and neither 16S rRNA sequencing nor culturing of CSE indicated the presence of any bacteria associated with CS-induced experimental COPD. Rather, dysbiosis is likely induced by products of CS such as nicotine and heavy metals that are present in circulation and accumulate in the gastrointestinal tract, directly influencing microbiota. 46 47 Additionally, we demonstrated that CS-associated microbiota suppressed local innate immune responses, including blunting TLR4 responses in vitro and reducing colonic innate immune populations such as microbiome-dependent tissue resident macrophages in vivo. 48 We previously reported opposing roles for lung TLR4 (pathogenic) and TLR2 (protective) in COPD¹⁸ and provide further evidence here that their signalling in the colon impacts pathogenesis, which is consistent with the protective effects of P. goldsteinii mediated by reduced activation of TLR4.11 Moreover, changes in TLR3, which recognises damage associated-molecular patterns, suggests an association with colonic pathology in COPD.⁴⁹ Given that long-term smoking is associated with colonic inflammation, the local immunosuppressive effects of CS-associated taxa may contribute to their persistence and expansion in these conditions, causing CS-induced dysbiosis while promoting lung inflammation that promotes disease progression.

In mice exposed to CS, FMT alleviated disturbances in systemic immunity including increased blood Ly6Clo (nonclassical) monocytes and depleted blood B cells and splenic CD8+ cDCs. Non-classical monocytes, associated with tissue repair or autoimmune damage, 50 are increased in severe COPD 51 and thus the FMT-mediated reduction is likely associated with the suppression of alveolar destruction. CD8+ cDCs, particularly in the spleen, are implicated in immune tolerance, phagocytosis and cross-presenting antigens, suggesting an association with increased blood B cells in FMT-treated mice. 52 Splenic cDC numbers are increased in models of acute lung injury,⁵³ demonstrating a spleen-lung axis regulated by gut microbiota. Restoration of systemic immune responses by FMT is consistent with evidence that FMT from air-exposed mice into naïve mice after antibiotic depletion did not deplete colonic immune cell populations as it did with FMT from CS-exposed mice. Restoration of colonic immune responses likely contributes to FMT-mediated reductions in Lachnospiraceae member UBA3282 sp009774575 and Mailhella sp003512875 in CS-exposed mice, but other mechanisms also contribute to protective effects including competitive relationships between bacteria. Most non-random relationships between bacteria were co-present relationships between groups of air-associated or CS-associated taxa, demonstrating that environmental conditions and exposures were the dominant influence on overall microbiome composition. However, multiple air/FMT-associated taxa had mutual exclusion relationships with Mailhella sp003512875, demonstrating that introduction of these species through FMT contributes to control of CS-associated species. Mutual exclusion with airassociated UBA7173 sp001689685 is particularly noteworthy, given it is negatively correlated with inflammation and emphysema and provides further evidence of protective effects mediated by mutual exclusion. Isolation and culture of these taxa will provide further insight into their relationship.

In the faecal proteome, increased chaperone protein DnaK (AELOFPMA_23737) and urease subunit alpha (GFDOOBDM_36378) after 12 weeks CS may be in response to heavy metals which rapidly reduce after smoking cessation. 46 54 55 Hydrolysis of urea by urease increases nitrogen availability, which has been linked to the persistence of deleterious bacteria and inflammation. 55

Alkyl hydroperoxide reductase GDJJNAEL 42303 and rubrerythrin BGMILIAL 35735 deactivate hydrogen peroxide to permit bacterial survival. 56 57 Increased alkyl hydroperoxide reductase in response to CS-induced oxidative stress³⁸ may explain the expansion of Desulfovibrionaceae that thrive in oxidative conditions,⁵⁸ and antioxidants are postulated to maintain the mucous barrier in patients with COPD.³⁸ That rubrerythrin was reduced by CS and increased by FMT indicates that the local environment influences oxidative stress responses and microbial adaptability. For example, rubrerythrin uses iron as a cofactor⁵⁶ whereas alkyl hydroperoxide reductase is repressed in high iron environments.⁵⁷ Many patients with COPD have iron deficiency³⁸ and lower hepcidin levels in CS-exposed mice increase absorption and reduce iron in the intestinal lumen,⁵ and may contribute to the different oxidative stress responses and expansion of pathogenic taxa in COPD.

Phosphoglycerate kinase AAEHAFLO_09769 and malate dehydrogenase EAAGGHIE_49748 are involved in glycolysis and gluconeogenesis⁶⁰ ⁶¹ and their abundance is increased in nutrient restriction, including by *Lachnospiraceae* spp.⁶⁰ ⁶¹ Nicotine is an appetite suppressant⁶² and reduced food consumption alters intestinal microbiota and predisposes to *Streptococcus pneumoniae* infection,³⁸ a major cause of COPD exacerbations and lung dysbiosis.⁵

Reduced abundance of microbial amino acid metabolites and increased secondary bile acids may be relevant for disease pathogenesis, particularly given recent evidence of a protective effect of the tryptophan metabolite indole-3-acetic acid in the airways⁶³ and the increasingly recognised role of bile acids as regulators of mucosal immunity.⁶⁴ Metabolomics also confirmed the disruption of carbohydrate metabolism identified by proteomic analysis that was selected for further investigation. Complex carbohydrates like resistant starch and inulin are poorly digested by the host, improving availability to microbiota stimulating anti-inflammatory short chain fatty acids(SCFAs). 6 38 High fibre intake is associated with lower risk of developing COPD,³⁸ and inulin reduced airway inflammation in asthma.⁶ Resistant starch reduced inflammation and emphysema in experimental COPD, and our pilot study in patients with COPD indicated that even a short period of inulin supplementation may reduce exacerbations and symptoms. However, examination of exacerbation frequency during the short period of intervention and assessment (4 weeks) should be interpreted with caution. Trials in larger cohorts of patients with COPD, and over longer periods of time, are needed to definitively demonstrate alleviation of symptoms and exacerbations and to progress these findings into clinical practice. While inulin is an established prebiotic in humans and improves translatability for future studies, 65 it is a different fibre to the resistant starch used in mice and therefore affects different bacterial populations. Resistant starch typically enriches Ruminococcus, Bifidobacterium, Faecalibacterium prausnitzii and Eubacterium rectale. Our study indicated that resistant starch increased one Bifidobacterium ASV which was negatively correlated with inflammation in mice. Inulin increases Bifidobacterium, Anaerostipes, Faecalibacterium and Lactobacillus, although there is significant variability between individuals and studies due to the baseline metabolic capacity of microbiota.66 67 Inulin primarily increased Bacteroides in our human cohort, which may indicate different responses to inulin supplements in patients with COPD compared with other cohorts, but the low sample size and high variability in both microbiome composition and prebiotic responses limits interpretation. Nevertheless, the anti-inflammatory effects of resistant starch associated with Bifidobacterium here, evidence of

probiotic *B. longum* in CS-induced inflammation²² and the established bifidogenic activity of inulin suggests greater efficacy of symbiotic *Bifidobacterium*-inulin supplements in COPD. Careful consideration of differences in microbial populations between animal models and patients with COPD, as well as between different cohorts of patients with COPD, will be required for future investigations in larger cohorts.

Jang et al showed limited evidence for FMT alleviating whole-body CS-exposure/poly I:C-induced emphysema which were associated, but not correlated, with increased Lactobacillaceae and decreased Bacteroidaceae identified through 16S rRNA gene sequencing. 10 Whole body CS-exposure coats the fur and grooming will unnaturally affect gut microbiota.⁶⁸ Without appropriate controls (no CS or poly I:C alone) and baseline microbiome normalisation or sampling, it was not possible to discern the different effects of CS and poly I:C, a TLR3 agonist, or determine whether changes in microbiota were due to confounding factors including cage effects, 42 accelerated ageing in COPD and the maturation of the microbiota, or the effects of PBS/saline vehicle gavage on gut microbiota, immune responses and lung histopathology. 41 That study was not translatable, as it did not assess the most clinically relevant feature of COPD (impaired lung function) or assess efficacy in humans. 10 The lack of human translation has been a limitation of other models of experimental COPD, 11 particularly given that experiments rarely consider the impacts in the context of smoking cessation, the current first-line treatment for COPD.

Our nose-only CS-exposures accurately reflects human exposures and disease mechanisms,⁴ and included microbiome normalisation, baseline microbiome assessment and demonstration of therapeutic benefits using FMT by both bedding swap and oral gavage to discriminate between disease-associated changes and those from confounding factors. Higher resolution metagenomic sequencing and correlation of individual taxa with disease features allowed species-level classification to elucidate the different, and sometimes contrasting, effects of family members such as CS-associated Amulumruptor sp001689515 and air/ FMT-associated M. intestinale and UBA7173 sp001689685 from the Muribaculaceae family. The efficacy of FMT was demonstrated in several contexts, including mild and severe disease, gastrointestinal comorbidities and providing additional benefits to smoking cessation by alleviating persistent increases in macrophages that drive progressive disease. 12 Translatability was enhanced by assessing lung function and extending our work in a pilot study to demonstrate clinically relevant alleviation of symptoms in patients. Overall, our study provides strong evidence for the therapeutic efficacy of FMT and complex carbohydrate supplementation which could be acceptable interventions for patients with COPD, that may become more effective when combined with smoking cessation. 65

A limitation of this and other studies is the lack of assessment of viral and fungal components of the microbiome in COPD. While their role in COPD has not been clarified, gastrointestinal fungi, especially *Candida*, have been implicated in lung cancer⁷⁰ and murine models of allergic airway disease along with changes in lung and gut innate immune cell populations. The Fungi and viruses also activate TLRs, including recognition of β -glucans by TLR2, O-linked mannans by TLR4, fungal/viral RNA by TLR3 and 7 and DNA by TLR9, and thus may overlap with several mechanisms identified in this study. Neither viral not fungal components could be confidently detected in our metagenomics data using read mapping to reference genomes or marker gene detection tools, likely due to the relatively shallow depth (~3 Gb). Even PCR amplification of the fungal ITS2

region did not yield sufficient material for adequate sequencing coverage, indicating low fungal abundance in our samples. Insufficient material for ITS2 sequencing can commonly occur in ~30% of faecal samples from mice and humans, ^{76 77} and faecal fungal abundance is lower in laboratory mice housed in clean conditions. Future studies should consider the introduction of wild microbiota to laboratory mice to improve capacity for investigation of fungal communities, and use deeper sequencing methods to investigate both fungal and viral components of the microbiota.

CONCLUSIONS

We demonstrate that dysbiosis, including increased *Muribaculaceae*, *Desulfovibrionaceae* and *Lachnospiraceae* species, contributes to disease pathogenesis and FMT alleviates hallmark features of CS-induced COPD. These changes may be affected by microbial energy metabolism, and complex carbohydrate supplementation protects against experimental disease and reduced exacerbations and symptoms in humans. This work opens new avenues towards effective microbiome-targeting therapies in COPD.

Author affiliations

¹Priority Research Centre for Healthy Lungs and Immune Health Research Program, The University of Newcastle and Hunter Medical Research Institute, Newcastle, NSW, Australia

²School of Chemistry and Molecular Biosciences, Australian Centre for Ecogenomics, The University of Queensland, Brisbane, QLD, Australia

³Centre for Inflammation, Centenary Institute, Sydney, NSW, Australia

⁴School of Life Sciences, Faculty of Science, University of Technology Sydney, Sydney, NSW, Australia

⁵UQ Thoracic Research Centre, Faculty of Medicine, The University of Queensland, Brisbane, QLD, Australia

⁶Department of Thoracic Medicine, The Prince Charles Hospital, Chermside, QLD, Australia

⁷Respiratory Bioinformatics and Molecular Biology, School of Life Sciences, University of Technology Sydney, NSW, Australia

⁸Frazer Institute, University of Queensland, Woolloongabba, QLD, Australia

⁹Sydney Cytometry, Charles Perkins Centre, Centenary Institute and The University of Sydney, Sydney, NSW, Australia

¹⁰Marie Bashir Institute for Infectious Diseases and Biosecurity, The University of Sydney, NSW, Australia

¹ Ramaciotti Facility for Human Systems Biology, Charles Perkins Centre and The University of Sydney, Sydney, NSW, Australia

¹²Discipline of Pathology, Faculty of Medicine and Health, School of Medical Sciences, The University of Sydney, Sydney, NSW, Australia

 13 Sydney Mass Spectrometry, The University of Sydney, Sydney, NSW, Australia
 14 School of Life and Environmental Sciences, Charles Perkins Centre and The University of Sydney, Sydney, NSW, Australia

¹⁵Systems Medicine, Deutsches Zentrum für Neurodegenerative Erkrankungen (DZNE), Bonn, Germany

¹⁶Genomics and Immunoregulation, Life & Medical Sciences (LIMES) Institute, University of Bonn, Bonn, Germany

¹⁷PRECISE Platform for Single Cell Genomics and Epigenomics, Deutsches Zentrum für Neurodegenerative Erkrankungen (DZNE) and the University of Bonn, Bonn, Germany

¹⁸Lydia Becker Institute of Immunology and Inflammation, University of Manchester, Manchester, IJK

¹⁹Centre for Innate Immunity and Infectious Diseases and Department of Molecular and Translational Science, Hudson Institute of Medical Research and Monash University, Melbourne, VIC, Australia

Institute for Molecular Bioscience, The University of Queensland, Brisbane, QLD,
 Australia
 Division of Pulmonary and Critical Care Medicine, Laura and Isaac Perlmutter

²¹Division of Pulmonary and Critical Care Medicine, Laura and Isaac Perlmutter Cancer Center, New York University Grossman School of Medicine, NYU Langone Health, New York, NY, USA

²²Lee Kong Chian School of Medicine, Translational Respiratory Research Laboratory,

Singapore ²³Mater Research Institute, Faculty of Medicine, University of Queensland, Brisbane, OLD. Australia

²⁴Department of Dietetics & Food Services, Mater Hospital, Brisbane, QLD, Australia
 ²⁵School of Earth and Environmental Sciences, The University of Queensland, Brisbane, QLD, Australia

Twitter Kurtis F Budden @KurtisBudden, Sj Shen @sjsijieshen, Nadia Amorim @ nadiamorim and Simon Keely @simonkeely

Acknowledgements We thank the Rainbow Foundation and Felicity and Michael Thomson for their support, Kristy Wheeldon, Emma Broadfield, Bradley Mitchell and Nathalie Kiaos for their help with animal models, and Nathan Smith for his help with proteomics analysis.

Contributors KFB, SDS, KLB, SLG, NGH, AV, TJH, EEH-W, EM, KMF, IAY, PH and PMH designed the study. KFB, SDS, SLG, SFR, CD, BT, NA, RM, CAA, KSV, JM, MF, TA, CvV, HMG and AV performed experiments. KFB, SDS, SLG, NIL, KSV and JM processed samples. KFB, SDS, KLB, SLG, DLAW, SI, VKP, AF, SFR, SS, KSV, TA, BC, SJC, LB, JLS, TA, BFdSG, NJCK and AV analysed the data. KFB, SDS, KLB, AV, TJH, LNS, SHC, IAY, SCF, PABW, PH and PMH interpreted the results. KFB, SDS, KLB, SI and AV prepared the manuscript. PMH is the guarantor for this paper. All authors edited and reviewed the manuscript.

Funding This work and PMH were supported by grants and fellowships from the National Health and Medical Research Council (NHMRC) of Australia (1059238, 1079187, 1175134), the Rainbow Foundation, Australian Research Council (1101107), Cancer Council of NSW, University of Newcastle and University of Technology Sydney and The Prince Charles Hospital Foundation (RF2017-05, INN2018-30). JLS was supported by German Research Foundation (DFG) under Germany's Excellence Strategy (EXC2151-390873048) as well as under SFB 1454 (432325352), the BMBF-funded excellence project Diet—Body—Brain (DietBB), EU grant under Horizon 2020 DiscovAir (874656) and the EU project SYSCID (733100).

Competing interests None declared.

Patient and public involvement Patients and/or the public were not involved in the design, or conduct, or reporting, or dissemination plans of this research.

Patient consent for publication Not applicable.

Ethics approval This study involves human participants and was approved by The Prince Charles Hospital Human Research Ethics Committee — HREC/18/QPCH/234. Participants gave informed consent to participate in the study before taking part.

Provenance and peer review Not commissioned; externally peer reviewed.

Data availability statement Data are available upon reasonable request. All data relevant to the study are included in the article or uploaded as supplementary information. Data are available on reasonable request. All data relevant to the study are included in the article or uploaded as online supplemental information. Shotgun metagenomics sequencing data for the microbiome of mice have been deposited in the NCBI BioProject database (https://www.ncbi.nlm.nih.gov/bioproject/) under accession number PRJNA740117 (https://dataview.ncbi.nlm.nih.gov/object/ PRJNA740117?reviewer=f8tgn1h6vsiqrfpnpiqt1r61i6) and may be re-used with appropriate acknowledgement. Raw data not included there can be obtained with the consent of the corresponding author.

Supplemental material This content has been supplied by the author(s). It has not been vetted by BMJ Publishing Group Limited (BMJ) and may not have been peer-reviewed. Any opinions or recommendations discussed are solely those of the author(s) and are not endorsed by BMJ. BMJ disclaims all liability and responsibility arising from any reliance placed on the content. Where the content includes any translated material, BMJ does not warrant the accuracy and reliability of the translations (including but not limited to local regulations, clinical guidelines, terminology, drug names and drug dosages), and is not responsible for any error and/or omissions arising from translation and adaptation or otherwise.

ORCID iDs

Kurtis F Budden http://orcid.org/0000-0002-7435-275X Shakti D Shukla http://orcid.org/0000-0002-5796-0171 Kate L Bowerman http://orcid.org/0000-0003-2339-114X Annalicia Vaughan http://orcid.org/0000-0001-5890-7877 Shaan L Gellatly http://orcid.org/0000-0002-7361-2337 David L A Wood http://orcid.org/0000-0002-1001-2019 Sobia Idrees http://orcid.org/0000-0001-8512-7593 Saima Firdous Rehman http://orcid.org/0000-0001-6269-355X Alen Faiz http://orcid.org/0000-0003-1740-3538 Chantal Donovan http://orcid.org/0000-0003-4558-329X Sj Shen http://orcid.org/0000-0002-1004-1936 Nadia Amorim http://orcid.org/0000-0002-3619-7410 Raiib Maiumder http://orcid.org/0000-0002-7244-6058 Kanth S Vanka http://orcid.org/0000-0003-3641-2499 Tatt Jhong Haw http://orcid.org/0000-0003-2315-7089 Bree Tillet http://orcid.org/0000-0002-0159-6649 Michael Fricker http://orcid.org/0000-0002-8587-1774 Simon Keely http://orcid.org/0000-0002-1248-9590 Nicole Hansbro http://orcid.org/0000-0002-2371-7990 Gabrielle T Belz http://orcid.org/0000-0002-9660-9587 Jay Horvat http://orcid.org/0000-0002-8526-0631

Gut microbiota

Thomas Ashhurst http://orcid.org/0000-0001-7269-7773 Caryn van Vreden http://orcid.org/0000-0003-4151-3470 Helen McGuire http://orcid.org/0000-0003-2047-6543 Barbara Fazekas de St Groth http://orcid.org/0000-0001-6817-9690 Nicholas J C King http://orcid.org/0000-0002-3877-9772 Ben Crossett http://orcid.org/0000-0001-5366-4554 Stuart J Cordwell http://orcid.org/0000-0002-0995-0171 Lorenzo Bonaguro http://orcid.org/0000-0001-9675-7208 Joachim L Schultze http://orcid.org/0000-0003-2812-9853 Emma E Hamilton-Williams http://orcid.org/0000-0003-4892-3691 Samuel C Forster http://orcid.org/0000-0003-4144-2537 Matthew A Cooper http://orcid.org/0000-0003-4144-2537 Leopoldo N Segal http://orcid.org/0000-0003-3559-9431 Peter Collins http://orcid.org/0000-0002-5273-8213 Kwun M Fong http://orcid.org/0000-0002-6507-1403 Ian A Yang http://orcid.org/0000-0001-8338-1993 Peter A B Wark http://orcid.org/0000-0001-5676-6126 Paul G Dennis http://orcid.org/0000-0002-4895-3105 Philip Hugenholtz http://orcid.org/0000-0001-5386-7925 Philip M Hansbro http://orcid.org/0000-0002-4741-3035

REFERENCES

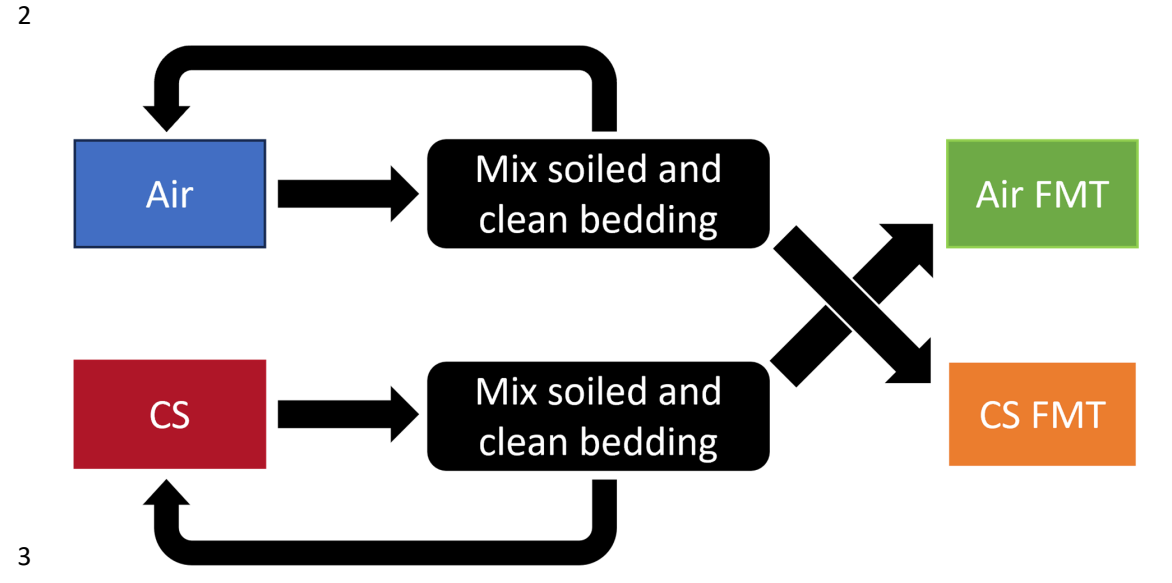
- 1 Agustí A, Celli BR, Criner GJ, et al. Global Initiative for Chronic Obstructive Lung Disease 2023 Report: GOLD Executive Summary. Eur Respir J 2023;61:2300239.
- 2 Safiri S, Carson-Chahhoud K, Noori M, et al. Burden of chronic obstructive pulmonary disease and its attributable risk factors in 204 countries and territories, 1990-2019: results from the Global Burden of Disease Study 2019. BMJ 2022:378:e060679
- 3 Halpin DMG, Criner GJ, Papi A, et al. Global Initiative for the Diagnosis, Management, and Prevention of Chronic Obstructive Lung Disease. Am J Respir Crit Care Med 2021:203:24–36.
- 4 Jones B, Donovan C, Liu G, et al. Animal models of COPD: What do they tell us? Respirology 2017;22:21–32.
- 5 Budden KF, Shukla SD, Rehman SF, et al. Functional effects of the microbiota in chronic respiratory disease. *Lancet Respir Med* 2019;7:907–20.
- 6 Budden KF, Gellatly SL, Wood DLA, et al. Emerging pathogenic links between microbiota and the gut-lung axis. Nat Rev Microbiol 2017;15:55–63.
- 7 Fricker M, Goggins BJ, Mateer S, et al. Chronic cigarette smoke exposure induces systemic hypoxia that drives intestinal dysfunction. JCI Insight 2018;3:e94040.
- 8 Bowerman KL, Rehman SF, Vaughan A, et al. Disease-associated gut microbiome and metabolome changes in patients with chronic obstructive pulmonary disease. Nat Commun 2020;11:5886.
- 9 Borody TJ, Eslick GD, Clancy RL. Fecal microbiota transplantation as a new therapy: from Clostridioides difficile infection to inflammatory bowel disease, irritable bowel syndrome, and colon cancer. Curr Opin Pharmacol 2019;49:43–51.
- 10 Jang YO, Lee SH, Choi JJ, et al. Fecal microbial transplantation and a high fiber diet attenuates emphysema development by suppressing inflammation and apoptosis. Exp Mol Med 2020;52:1128–39.
- 11 Lai H-C, Lin T-L, Chen T-W, et al. Gut microbiota modulates COPD pathogenesis: role of anti-inflammatory Parabacteroides goldsteinii lipopolysaccharide. Gut 2022:71:309–21
- 12 Beckett EL, Stevens RL, Jarnicki AG, et al. A new short-term mouse model of chronic obstructive pulmonary disease identifies A role for mast cell tryptase in pathogenesis. J Allergy Clin Immunol 2013;131:752–62.
- 13 Starkey MR, Plank MW, Casolari P, et al. IL-22 and its receptors are increased in human and experimental COPD and contribute to pathogenesis. Eur Respir J 2019;54:1800174.
- 14 Prihandoko R, Kaur D, Wiegman CH, et al. Pathophysiological regulation of lung function by the free fatty acid receptor FFA4. Sci Transl Med 2020;12:eaaw9009.
- 15 Schanin J, Gebremeskel S, Korver W, et al. A monoclonal antibody to Siglec-8 suppresses non-allergic airway inflammation and inhibits IgE-independent mast cell activation. Mucosal Immunol 2021;14:366–76.
- 16 Cooper GE, Mayall J, Donovan C, et al. Antiviral Responses of Tissue-resident CD49a⁺ Lung Natural Killer Cells Are Dysregulated in Chronic Obstructive Pulmonary Disease. Am J Respir Crit Care Med 2023;207:553–65.
- 17 Tu X, Kim RY, Brown AC, et al. Airway and parenchymal transcriptomics in a novel model of asthma and COPD overlap. J Allergy Clin Immunol 2022;150:817–29.
- 18 Haw TJ, Starkey MR, Pavlidis S, et al. Toll-like receptor 2 and 4 have opposing roles in the pathogenesis of cigarette smoke-induced chronic obstructive pulmonary disease. Am J Physiol Lung Cell Mol Physiol 2018;314:L298–317.
- 19 Lu Z, Eeckhoutte HP, Liu G, et al. Necroptosis Signalling Promotes Inflammation, Airway Remodelling and Emphysema in COPD. Am J Respir Crit Care Med 2021;204:667–81.
- 20 Skerrett-Byrne DA, Bromfield EG, Murray HC, et al. Time-resolved proteomic profiling of cigarette smoke-induced experimental chronic obstructive pulmonary disease. Respirology 2021;26:960–73.

- 21 Scott NA, Andrusaite A, Andersen P, et al. Antibiotics induce sustained dysregulation of intestinal T cell immunity by perturbing macrophage homeostasis. Sci Transl Med 2018;10:eaao4755.
- 22 Budden KF, Gellatly SL, Vaughan A, et al. Probiotic Bifidobacterium longum subsp. longum Protects against Cigarette Smoke-Induced Inflammation in Mice. IJMS 2022:24:252.
- 23 Caporaso JG, Kuczynski J, Stombaugh J, et al. QIIME allows analysis of highthroughput community sequencing data. Nat Methods 2010;7:335–6.
- 24 Oksanen J, Blanchet FG, Kindt R, et al. Vegan: community Ecology package (R package version 23-1).
- 25 Paulson JN, Stine OC, Bravo HC, et al. Differential abundance analysis for microbial marker-gene surveys. Nat Methods 2013;10:1200–2.
- 26 Rohart F, Gautier B, Singh A, et al. mixOmics: An R package for 'omics feature selection and multiple data integration. PLOS Comput Biol 2017;13:e1005752.
- 27 Revelle W. Psych: procedures for personality and psychological research (R package version 1812).
- 28 Faust K, Raes J. CoNet app: inference of biological association networks using Cytoscape. F1000Res 2016;5:1519.
- 29 Parks DR, Roederer M, Moore WA. A new "Logicle" display method avoids deceptive effects of logarithmic scaling for low signals and compensated data. Cytometry A 2006;69:541–51.
- 30 Levine JH, Simonds EF, Bendall SC, et al. Data-Driven Phenotypic Dissection of AML Reveals Progenitor-like Cells that Correlate with Prognosis. Cell 2015;162:184–97.
- 31 Washburn MP. The H-index of "an approach to correlate tandem mass spectral data of peptides with amino acid sequences in a protein database." J Am Soc Mass Spectrom 2015;26:1799–803.
- 32 Xiao L, Feng Q, Liang S, et al. A catalog of the mouse gut metagenome. Nat Biotechnol 2015;33:1103–8.
- 33 Bailey JM, Blanchard R, Hsu KJ, et al. A map of desire: multidimensional scaling of men's sexual interest in male and female children and adults. Psychol Med 2021;51:2714–20.
- 34 Parks DH, Chuvochina M, Chaumeil P-A, et al. A complete domain-to-species taxonomy for Bacteria and Archaea. Nat Biotechnol 2020;38:1079–86.
- 35 Larsson L, Pehrson C, Dechen T, et al. Microbiological components in mainstream and sidestream cigarette smoke. Tob Induc Dis 2012;10:13.
- 36 Malayil L, Chattopadhyay S, Bui A, et al. Viable bacteria abundant in cigarettes are aerosolized in mainstream smoke. Environ Res 2022;212:113462.
- 37 Beresford-Jones BS, Forster SC, Stares MD, et al. The Mouse Gastrointestinal Bacteria Catalogue enables translation between the mouse and human gut microbiotas via functional mapping. Cell Host Microbe 2022;30:124–38.
- 38 Alemao CA, Budden KF, Gomez HM, et al. Impact of diet and the bacterial microbiome on the mucous barrier and immune disorders. Allergy 2021:76:714–34.
- 39 Kon SSC, Canavan JL, Jones SE, et al. Minimum clinically important difference for the COPD Assessment Test: a prospective analysis. Lancet Respir Med 2014;2:195–203.
- 40 Gheorghe CE, Ritz NL, Martin JA, et al. Investigating causality with fecal microbiota transplantation in rodents: applications, recommendations and pitfalls. Gut Microbes 2021:13:1941711.
- 41 Larcombe AN, Wang KCW, Phan JA, et al. Confounding Effects of Gavage in Mice: Impaired Respiratory Structure and Function. Am J Respir Cell Mol Biol 2019;61:791–4.
- 42 Dickson RP, Erb-Downward JR, Falkowski NR, et al. The Lung Microbiota of Healthy Mice Are Highly Variable, Cluster by Environment, and Reflect Variation in Baseline Lung Innate Immunity. Am J Respir Crit Care Med 2018;198:497–508.
- 43 Li N, Dai Z, Wang Z, et al. Gut microbiota dysbiosis contributes to the development of chronic obstructive pulmonary disease. Respir Res 2021;22:274.
- 44 Li N, Yi X, Chen C, et al. The gut microbiome as a potential source of non-invasive biomarkers of chronic obstructive pulmonary disease. Front Microbiol 2023;14:1173614.
- 45 Lee SH, Kim J, Kim NH, et al. Gut microbiota composition and metabolite profiling in smokers: a comparative study between emphysema and asymptomatic individuals with therapeutic implications. *Thorax* 2023;78:1080–9.
- 46 Prokopowicz A, Sobczak A, Szuła-Chraplewska M, et al. Exposure to Cadmium and Lead in Cigarette Smokers Who Switched to Electronic Cigarettes. Nicotine Tob Res 2019;21:1198–205.
- 47 Chen B, Sun L, Zeng G, et al. Gut bacteria alleviate smoking-related NASH by degrading gut nicotine. Nature 2022;610:562–8.
- 48 Shaw TN, Houston SA, Wemyss K, et al. Tissue-resident macrophages in the intestine are long lived and defined by Tim-4 and CD4 expression. J Exp Med 2018:215:1507–18.
- 49 Vontell R, Supramaniam V, Wyatt-Ashmead J, et al. Cellular mechanisms of toll-like receptor-3 activation in the thalamus are associated with white matter injury in the developing brain. J Neuropathol Exp Neurol 2015;74:273–85.
- 50 Yang J, Zhang L, Yu C, et al. Monocyte and macrophage differentiation: circulation inflammatory monocyte as biomarker for inflammatory diseases. Biomark Res 2014:2:1.
- 51 Cornwell WD, Kim V, Fan X, et al. Activation and polarization of circulating monocytes in severe chronic obstructive pulmonary disease. BMC Pulm Med 2018;18:101.

- 52 Shortman K, Heath WR. The CD8+ dendritic cell subset. *Immunol Rev* 2010:234:18–31.
- 53 Liu J, Zhang PS, Yu Q, et al. Kinetic and distinct distribution of conventional dendritic cells in the early phase of lipopolysaccharide-induced acute lung injury. Mol Biol Rep 2012;39:10421–31.
- 54 Keller-Costa T, Lago-Lestón A, Saraiva JP, et al. Metagenomic insights into the taxonomy, function, and dysbiosis of prokaryotic communities in octocorals. Microbiome 2021:9:72.
- 55 Kelley BR, Lu J, Haley KP, et al. Metal homeostasis in pathogenic Epsilonproteobacteria: mechanisms of acquisition, efflux, and regulation. Metallomics 2021:13:mfaa002.
- 56 Lumppio HL, Shenvi NV, Summers AO, et al. Rubrerythrin and rubredoxin oxidoreductase in Desulfovibrio vulgaris: a novel oxidative stress protection system. J Bacteriol 2001;183:101–8.
- 57 Pinochet-Barros A, Helmann JD. Redox Sensing by Fe(2+) in Bacterial Fur Family Metalloregulators. *Antioxid Redox Signal* 2018;29:1858–71.
- 58 Van Hecke T, De Vrieze J, Boon N, et al. Combined Consumption of Beef-Based Cooked Mince and Sucrose Stimulates Oxidative Stress, Cardiac Hypertrophy, and Colonic Outgrowth of Desulfovibrionaceae in Rats. Molecular Nutrition Food Res 2019:63.
- 59 Perez E, Baker JR, Di Giandomenico S, et al. Hepcidin Is Essential for Alveolar Macrophage Function and Is Disrupted by Smoke in a Murine Chronic Obstructive Pulmonary Disease Model. J Immunol 2020;205:2489–98.
- 60 Breton J, Legrand R, Achamrah N, et al. Proteome modifications of gut microbiota in mice with activity-based anorexia and starvation: Role in ATP production. *Nutrition* 2019:67–68:110557.
- 61 Bruffaerts N, Vluggen C, Roupie V, et al. Virulence and immunogenicity of genetically defined human and porcine isolates of M. PLoS One 2017;12:E0171895.
- 62 Courtemanche C, Tchernis R, Ukert B. The effect of smoking on obesity: Evidence from a randomized trial. J Health Econ 2018;57:31–44.
- 63 Yan Z, Chen B, Yang Y, et al. Multi-omics analyses of airway host-microbe interactions in chronic obstructive pulmonary disease identify potential therapeutic interventions. Nat Microbiol 2022;7:1361–75.
- 64 Chen ML, Takeda K, Sundrud MS. Emerging roles of bile acids in mucosal immunity and inflammation. *Mucosal Immunol* 2019;12:851–61.

- 65 Halnes I, Baines KJ, Berthon BS, et al. Soluble Fibre Meal Challenge Reduces Airway Inflammation and Expression of GPR43 and GPR41 in Asthma. Nutrients 2017;9:57.
- 66 Le Bastard Q, Chapelet G, Javaudin F, et al. The effects of inulin on gut microbial composition: a systematic review of evidence from human studies. Eur J Clin Microbiol Infect Dis 2020;39:403–13.
- 67 Bendiks ZA, Knudsen KEB, Keenan MJ, et al. Conserved and variable responses of the gut microbiome to resistant starch type 2. Nutr Res 2020;77:12–28.
- 68 Chun LF, Moazed F, Calfee CS, et al. Pulmonary toxicity of e-cigarettes. Am J Physiol Lung Cell Mol Physiol 2017;313:L193–206.
- 69 Vaughan A, Frazer ZA, Hansbro PM, et al. COPD and the gut-lung axis: the therapeutic potential of fibre. J Thorac Dis 2019;11(Suppl 17):S2173–80.
- 70 Seelbinder B, Lohinai Z, Vazquez-Uribe R, et al. Candida expansion in the gut of lung cancer patients associates with an ecological signature that supports growth under dysbiotic conditions. Nat Commun 2023;14:2673.
- 71 Kanj AN, Kottom TJ, Schaefbauer KJ, et al. Dysbiosis of the intestinal fungal microbiota increases lung resident group 2 innate lymphoid cells and is associated with enhanced asthma severity in mice and humans. Respir Res 2023;24:144.
- 72 Li X, Leonardi I, Semon A, et al. Response to Fungal Dysbiosis by Gut-Resident CX3CR1⁺ Mononuclear Phagocytes Aggravates Allergic Airway Disease. Cell Host Microbe 2018;24:847–56.
- 73 Bourgeois C, Kuchler K. Fungal pathogens-a sweet and sour treat for toll-like receptors. Front Cell Infect Microbiol 2012;2:142.
- 74 Liu G, Haw TJ, Starkey MR, et al. TLR7 promotes smoke-induced experimental lung damage through the activity of mast cell tryptase. Nat Commun 2023;14:7349.
- 75 Galloway-Peña J, Hanson B. Tools for Analysis of the Microbiome. *Dig Dis Sci* 2020:65:674–85.
- 76 Jones J, Reinke SN, Ali A, et al. Fecal sample collection methods and time of day impact microbiome composition and short chain fatty acid concentrations. Sci Rep 2021;11:13964.
- 77 Hoggard M, Vesty A, Wong G, et al. Characterizing the Human Mycobiota: A Comparison of Small Subunit rRNA, ITS1, ITS2, and Large Subunit rRNA Genomic Targets. Front Microbiol 2018;9:2208.
- 78 Yeung F, Chen Y-H, Lin J-D, et al. Altered Immunity of Laboratory Mice in the Natural Environment Is Associated with Fungal Colonization. Cell Host Microbe 2020;27:809–22.

1 Supplementary Figures:



- 4 Figure S1: Schematic of fecal microbial transfer (FMT) methodology. To administer FMT,
- 5 soiled bedding from air-exposed mice was mixed with clean bedding (1:2 ratio) and transferred to
- 6 the cages of smoke-exposed mice. Conversely, the soiled bedding from 12-week CS-exposed mice
- 7 was mixed with clean bedding and transferred to the cages of air-exposed mice. Control groups
- 8 (without FMT) received their own soiled bedding mixed with clean bedding.

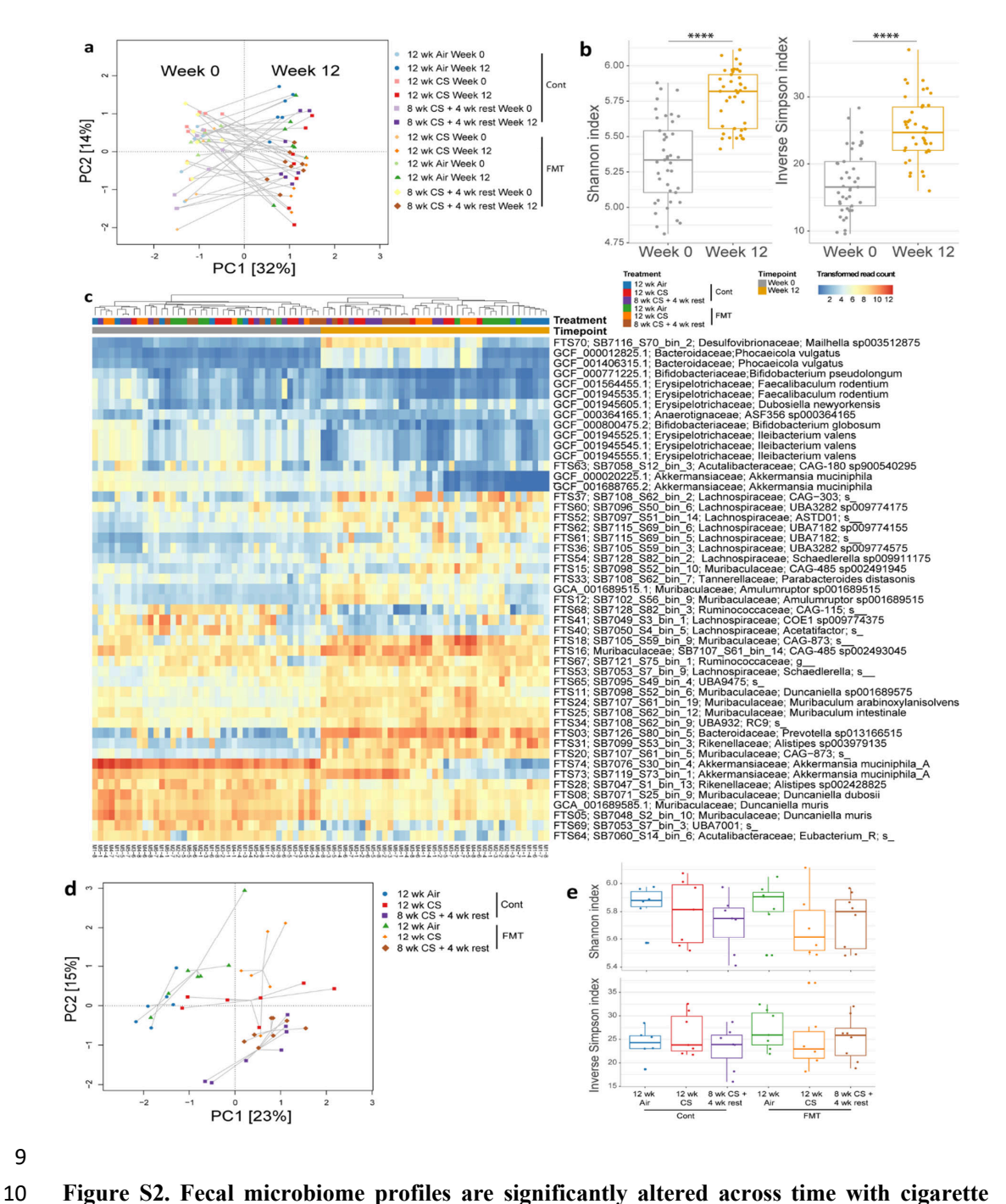


Figure S2. Fecal microbiome profiles are significantly altered across time with cigarette smoke (CS)-exposure and fecal microbiota treatment (FMT). a-e, Mice were exposed to CS (12 wk CS) or normal air (Air) for 12 weeks, or 8 weeks CS followed by 4 weeks with normal air

(8 wk CS+ 4 wk rest). Mice also received FMT through transfer of soiled bedding twice per week or were maintained in their own bedding (Control) for 12 weeks. Fecal samples from baseline (week 0) and at the end of the experiment (week 12) were analyzed using shotgun metagenomics. (a) Principal component analysis of all mice demonstrated shifts in microbiome composition with time, smoke-exposure and FMT based on genome level read mapping counts, log-cumulative-sum-scaling (CSS) transformed. (b) Simpson and Shannon diversity indices for all mice demonstrated increasing diversity over time based on mapping counts across all genomes transformed using the DESeq2 scaling factor. (c) Heatmap displaying significantly different genomes (Benjamini-Hochberg adjusted P<0.001, log2 fold change >1.5) between week 0 and week 12 as log-CSS transformed read counts. (d) Principal component analysis of week 12 mice demonstrated significant separation between groups using PERMANOVA of Bray-Curtis distances. (e) Simpson and Shannon diversity indices indicating no differences in diversity between experimental groups at week 12. N = 8 per group. **** = p<0.0001 using a Wilcoxon rank sum test.

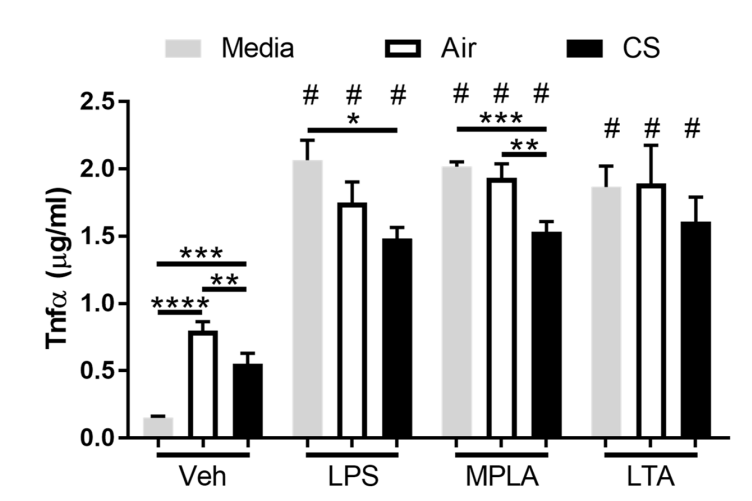


Figure S3: Cigarette smoke (CS)-induced dysbiosis impaired TLR4 agonist-induced TNFα production in monocytes. Raw 264.7 monocytes were incubated for 24 hours with sterile-filtered faecal homogenates from mice exposed to CS (black) or normal air (white) for 12 weeks, or were maintained in media (grey). In the last 4 hours of incubation, cells were incubated with lipopolysaccharide (LPS), monophosphoryl lipid A (MPLA), lipoteichoic acid (LTA) or vehicle (Veh; 0.5% dimethylsulfoxide). Incubation with faecal homogenates induced TNFα production, which was lower with faeces from CS-exposed mice. LPS- and MPLA-induced TNFα production was also lower in cells incubated with faeces from CS-exposed mice. N = 3-9 per group. Data presented as mean +/- standard error of the mean. ** = p<0.01; *** = p<0.001; **** = p<0.0001; *** = p<0.0001; *** = p<0.0001; *** = p<0.0001; *** = p<0.0001; **

43

44

45

46

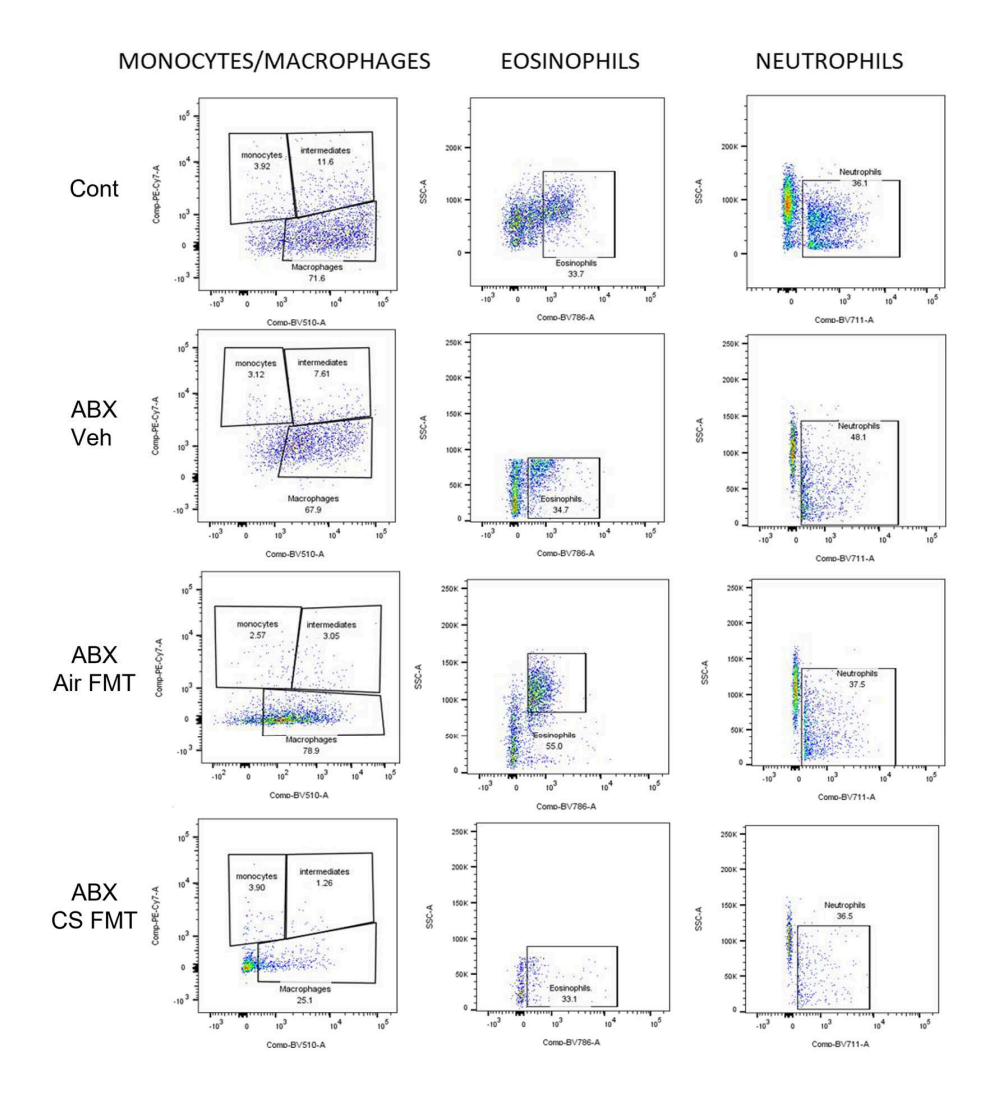


Figure S4: Representative FACS plots of colon granulocytes from Figure 5. Microbiota were depleted by antibiotics (ABX) for 7 days before mice were recolonized with feces from separate air- (Air FMT) or CS-exposed donors (CS FMT) for 10 days. A subset of mice received vehicle (Veh, PBS + 0.05% L-cysteine) to model natural recolonisation. Innate immune cells in the colon were enumerated by flow cytometry, with representative FACS plots displayed here.

50

51

52

53

EOSINOPHILS MONOCYTES INTERSTITIAL MACROPHAGES

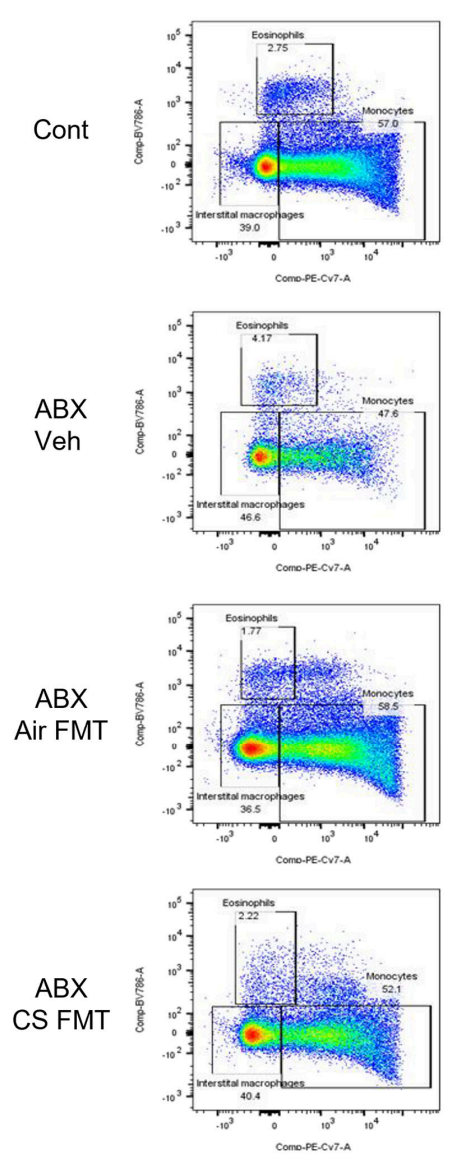


Figure S5: Representative FACS plots of colon granulocytes from Figure 5. Microbiota were depleted by antibiotics (ABX) for 7 days before mice were recolonized with feces from separate air- (Air FMT) or CS-exposed donors (CS FMT) for 10 days. A subset of mice received vehicle (Veh, PBS + 0.05% L-cysteine) to model natural recolonisation. Innate immune cells in the lung were enumerated by flow cytometry, with representative FACS plots displayed here.

55

56

57

58

59

60

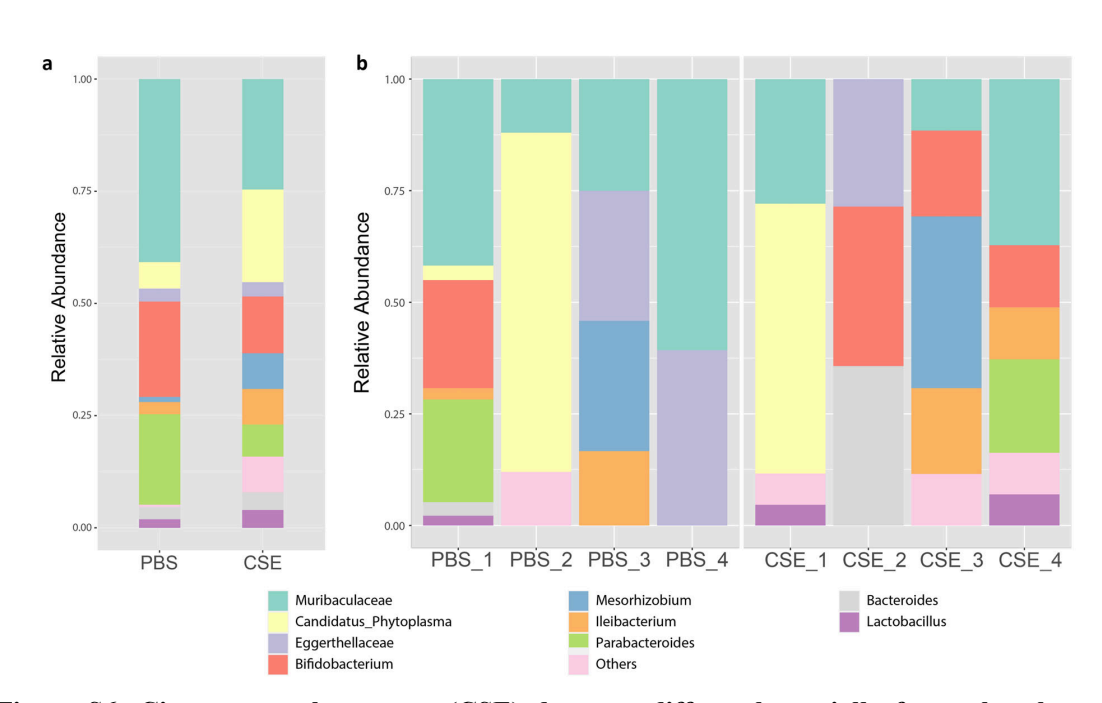


Figure S6: Cigarette smoke extract (CSE) does not differ substantially from phosphate buffered saline (PBS) negative control. CSE generated from 3R4F research cigarettes was assessed by 16S rRNA gene sequencing. (a) Overall composition did not differ substantially from negative controls and no cigarette smoke-associated taxa were identified in CSE above levels in negative controls. (b) There was significant variability in presence of bacterial genera between samples. N=4.

64

65

66

67

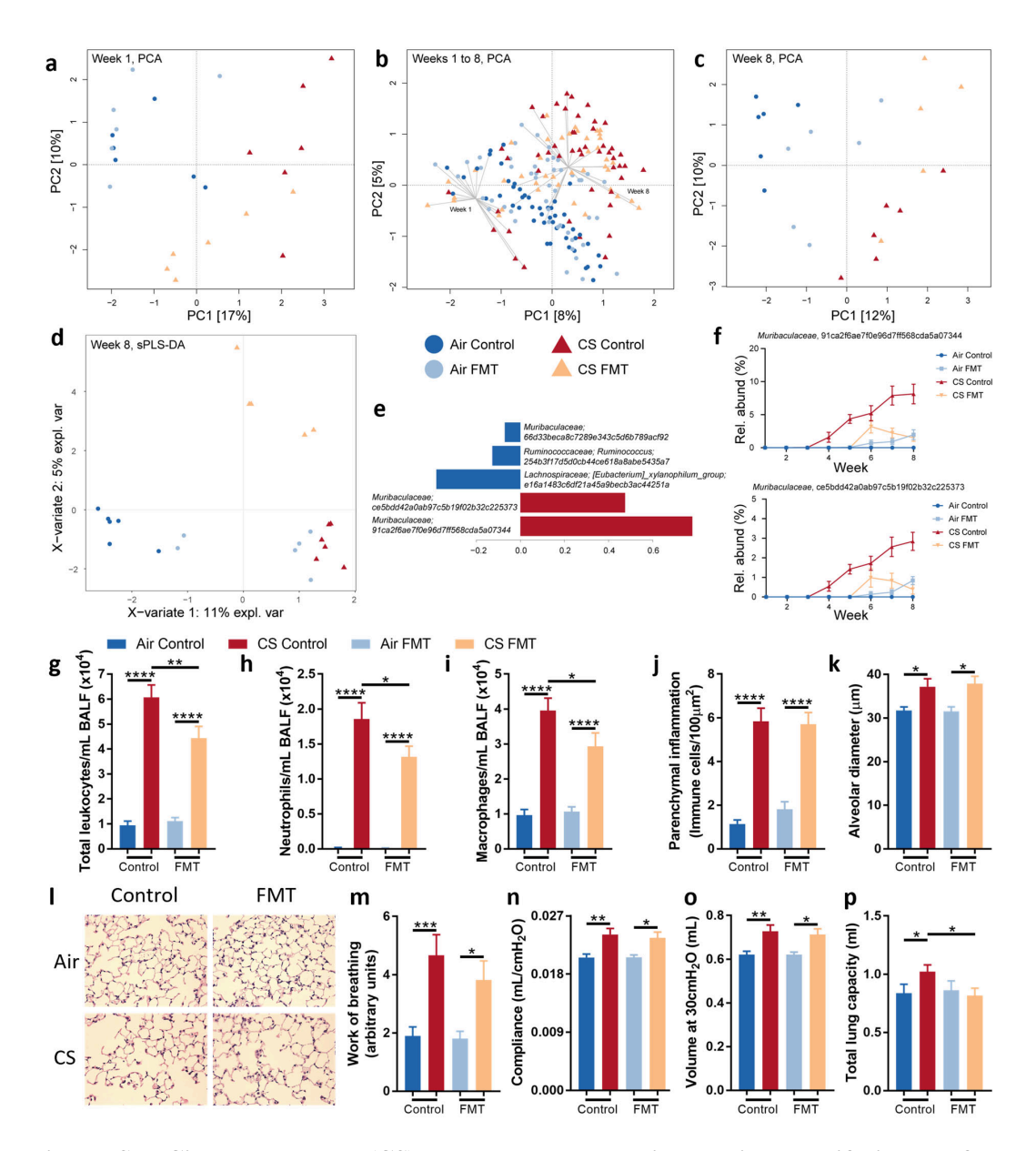


Figure S7. Cigarette smoke (CS)-exposure was associated with a shift in the faecal microbiome, and faecal microbiota transfer (FMT) suppressed the development of experimental COPD. Mice were exposed to CS or normal air for eight weeks and received FMT through transfer of soiled bedding or were maintained in their own bedding (Control). a-f, Faecal samples were collected weekly and analyzed by 16S rRNA amplicon sequencing. (a) Principal component analysis of mice following one week of CS-exposure and/or FMT, across (b) all eight

69 weeks of the experiment and at (c) week eight following completion of the experiment 70 demonstrated a clear distinction in microbiota composition of the different experimental groups. 71 (d) Multivariate analysis (sPLS-DA) at week eight demonstrated distinction between air- and CS-72 exposed groups along component 1, (e) with several species contributing to this separation. (f) 73 Relative abundance of Muribaculaceae sequence variants increased in CS-exposed mice but was 74 alleviated by FMT, contributing to separation of sPLS-DA across the eight-week experiment. g-p, 75 Hallmark features of COPD assessed at week eight. CS-exposure increased (g-i) total leukocytes, 76 neutrophils and macrophages in bronchoalveolar lavage fluid (BALF), (j) immune cells in 77 parenchyma, (k-l) alveolar diameter, and (m-p) lung function parameters of work of breathing, 78 compliance, volume and total lung capacity. FMT alleviated CS-induced increases in BALF total 79 leukocyte, neutrophil and macrophage numbers and total lung capacity. N = 5-6 per group (a-f) or 14-18 per group from 3 independent experiments (g-p). Data presented as mean +/- standard 80 error of the mean. * = p<0.05; ** = p<0.01; **** = p<0.001; ***** = p<0.0001 using one-way 81 82 ANOVA with Holm-Sidak's post-hoc analysis (g-p).

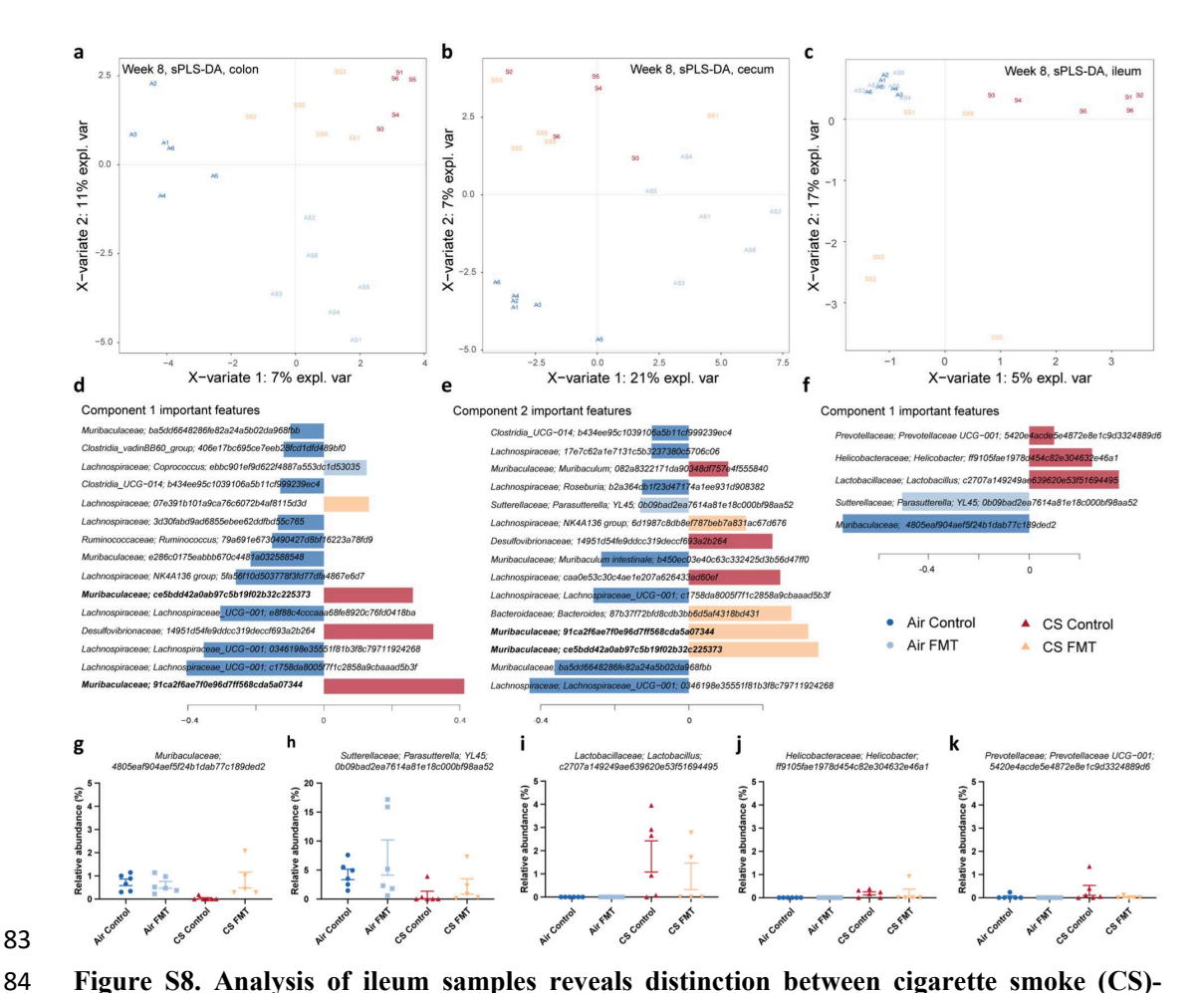


Figure S8. Analysis of ileum samples reveals distinction between cigarette smoke (CS)-exposed groups based on faecal microbiota transfer (FMT) treatment. a-k, Mice were exposed to CS or normal air (Air) for eight weeks, and received FMT through transfer of soiled bedding or were maintained in their own bedding (Control). Multivariate analysis (sPLS-DA) at week eight based on 16S rRNA amplicon sequencing indicated CS-induced separation of microbiome samples, resembling that observed in faecal samples, in the (a) colon and (b) caecum but not the (c) ileum, although the latter did demonstrate a difference between CS control and CS FMT groups.

(d) Species contributing to separation along the CS-associated component 1 of a and (e) component 2 of b. (f) Species contributing to separation along the air-associated component 1 of c. (g-k) Relative abundance of air-associated ASVs from the ileum from CS FMT mice trended towards the levels of air-exposed control mice. N = 5-6 per group.

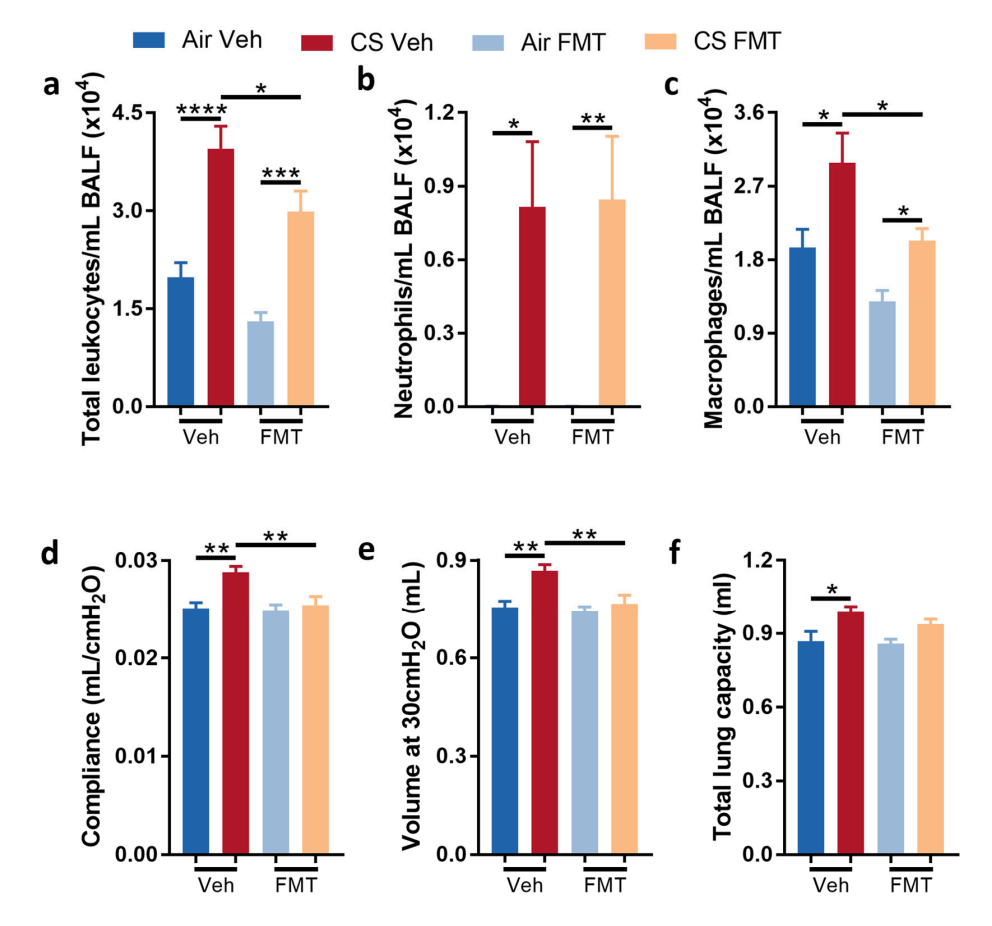


Figure S9. Faecal microbiota transfer (FMT) by oral gavage suppressed the development of experimental COPD. a-f, Mice were exposed to cigarette smoke or normal air for eight weeks and received FMT or vehicle (Veh; phosphate buffered saline + 0.05% L-cysteine) through oral gavage. (a-c) CS-exposure increased total leukocytes, neutrophils and macrophages numbers in bronchoalveolar lavage fluid (BALF), and (d-f) the lung function parameters compliance, volume and total lung capacity. FMT alleviated CS-induced increases in BALF total leukocytes and macrophages, and lung compliance and volume. N = 10-12 per group from 2 independent experiments. Data presented as mean +/- standard error of the mean. * = p < 0.05; ** = p < 0.01; **** = p < 0.001; **** = p < 0.0001 using one-way ANOVA with Holm-Sidak's post-hoc analysis.

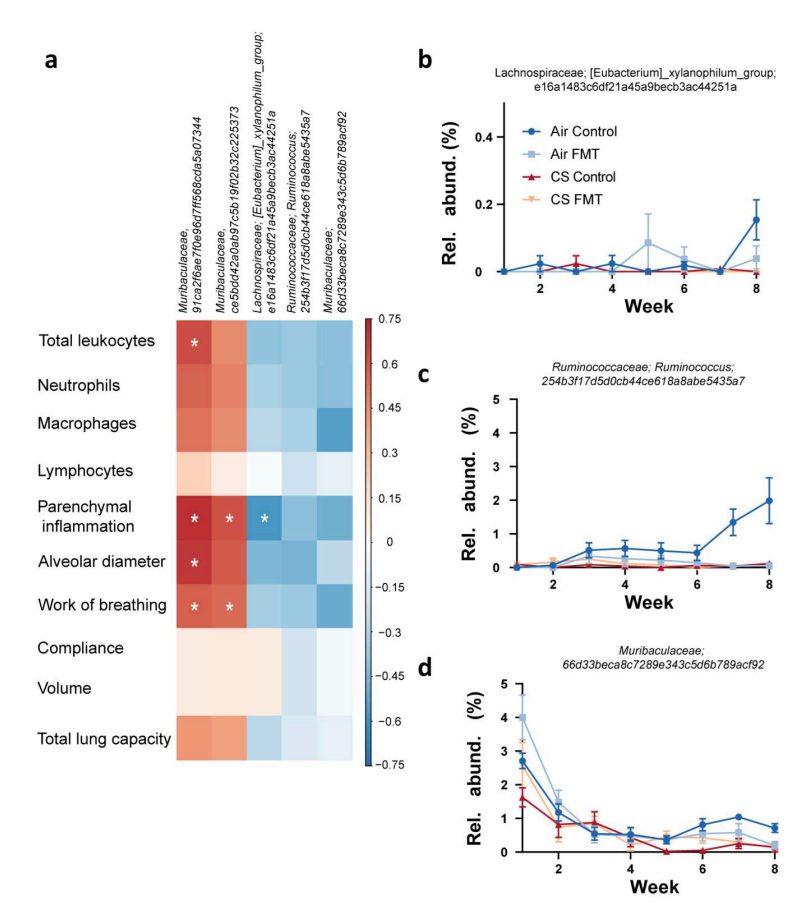


Figure S10: A cigarette smoke (CS)-associated *Muribaculaceae* amplicon sequence variant (ASV) correlates with a subset of phenotypic measures. a-d, Mice were exposed to CS or normal air (Air) for eight weeks and received faecal microbiota transfer (FMT) through transfer of soiled bedding or were maintained in their own bedding (Control). Faecal samples were collected weekly and analyzed by 16S rRNA amplicon sequencing. (a) Spearman's rho calculated between centered log-ratio transformed ASV relative abundance and phenotypic scores indicated correlation between *Muribaculaceae 91ca*. and a subset of phenotypic measures. (b-d) Relative abundances of air-associated ASVs from Fig. S2e across the eight-week experiment were variable. N = 5-6 per group. * = p<0.05 using Spearman's correlation.

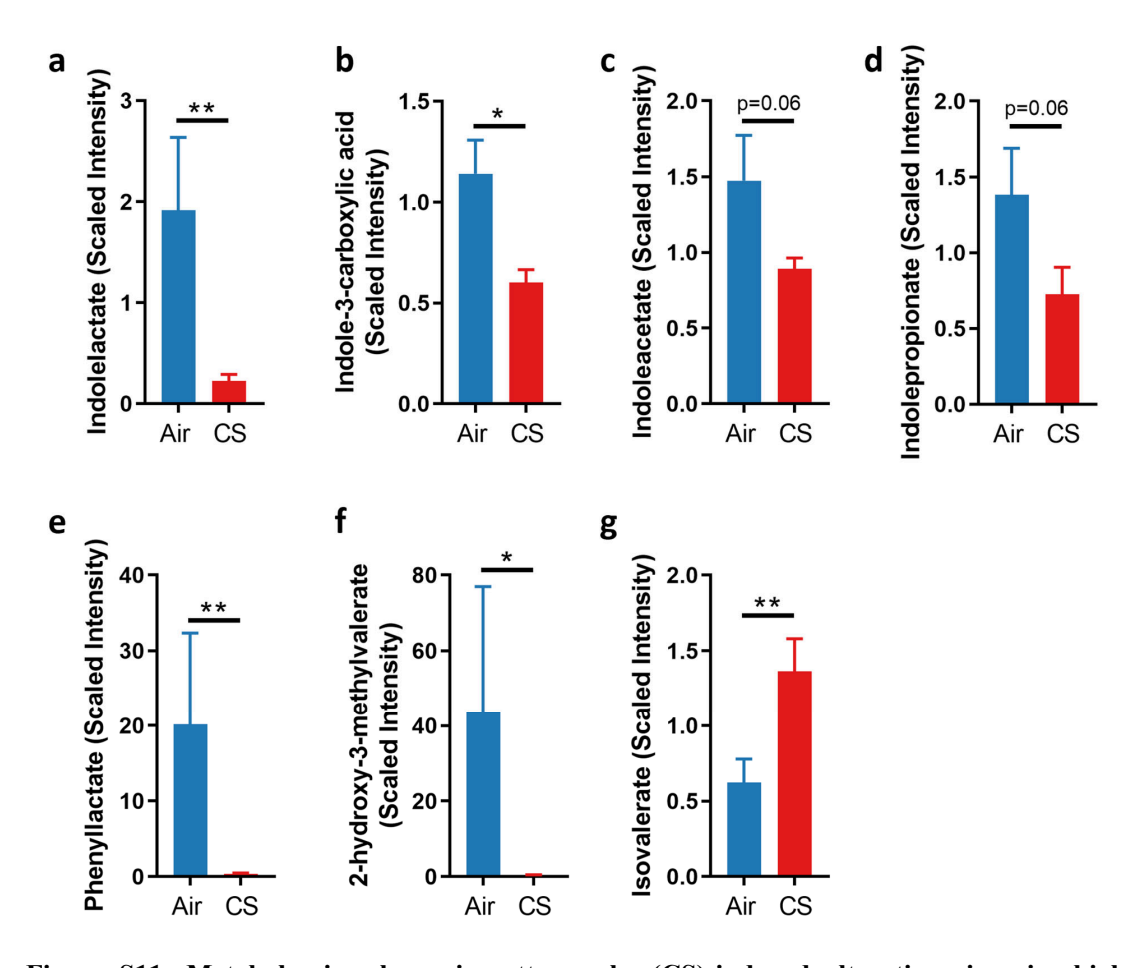


Figure S11: Metabolomics show cigarette smoke (CS)-induced alterations in microbial protein metabolism. a-g, Mice were exposed to CS or air for 12 weeks, and metabolites in cecum contents assessed. Microbial amino acid metabolites were broadly downregulated in response to CS, except for isovalerate which was increased. N = 8 per group. Data presented as mean +/-standard error of the mean. * = p<0.05; ** = p<0.01 using one-way unpaired Student's T test on log-transformed data.

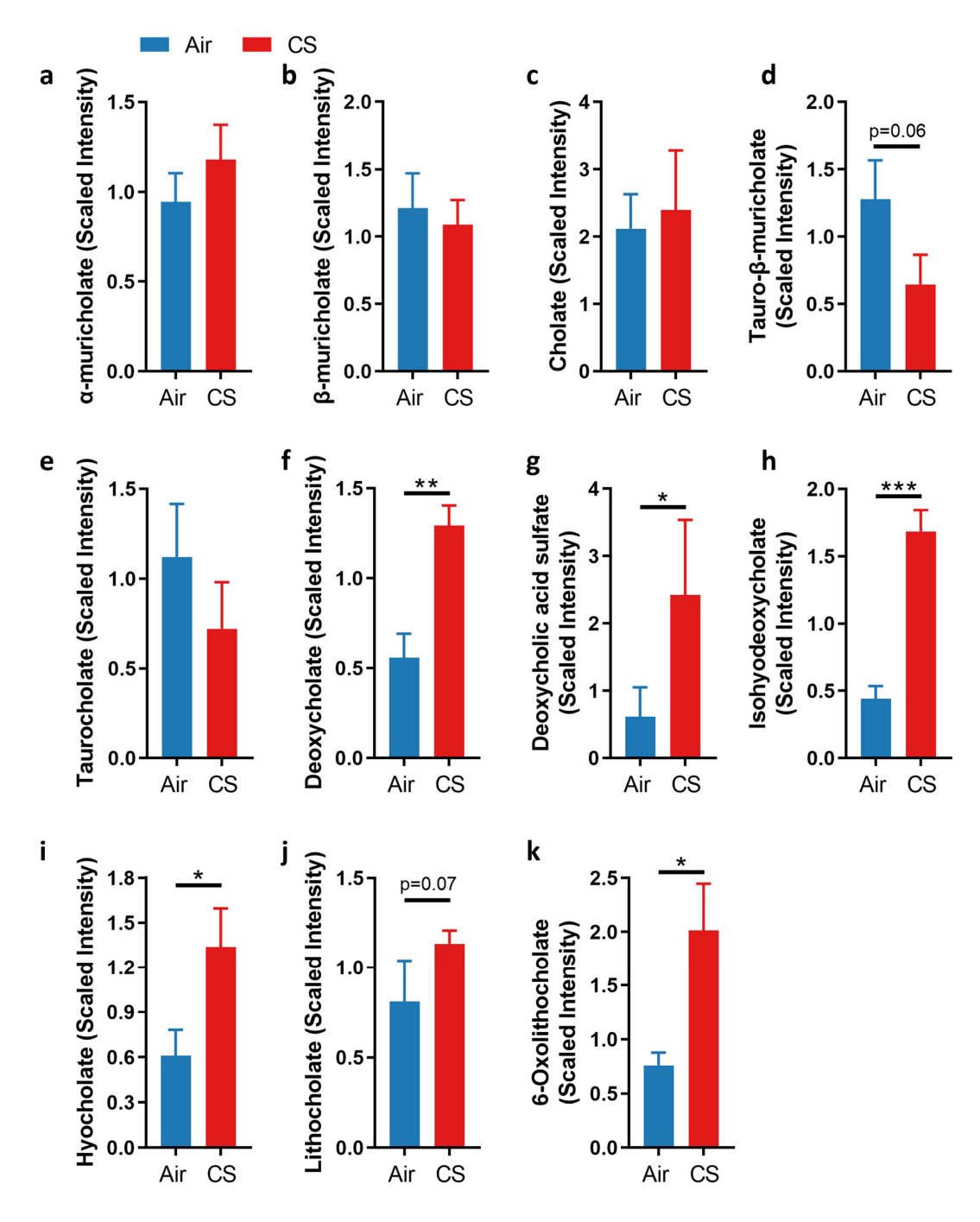


Figure S12: Metabolomics show cigarette smoke (CS)-induced alterations in microbial protein metabolism. a-k, Mice were exposed to CS or air for 12 weeks, and metabolites in cecum

134

135

136137138139140

contents assessed. (a-e) Host-derived primary bile acids were not altered by CS. (f-k) Secondary bile acids, produced by microbial metabolism of primary bile acids, were increased by CS. N=8 per group. Data presented as mean +/- standard error of the mean. * = p<0.05; ** = p<0.01; *** = p<0.001 using one-way unpaired Student's T test on log-transformed data.

142

144

145

146

147

149

152153

154

155

156

157

160

163

164

165

166

Supplementary Methods:

Mice, CS-exposure, microbiome transfer and diet studies

143 Female C57BL/6 mice (3-5 weeks old) were obtained from the Animal Services Unit, The

University of Newcastle (Newcastle, Australia). Upon arriving in the facility, the baseline

microbiome was normalized for three weeks by pooling and mixing all soiled bedding and

redistributing to all cages (twice weekly) and co-housing mice from different experimental groups

weekly. Microbiome normalization was not performed for validation experiments (8 weeks CS

148 with FMT).

150 Mice were exposed to normal room air or CS from twelve 3R4F reference cigarettes (University

of Kentucky, Lexington, KY) in a custom-designed, nose-only inhalation apparatus, twice per day,

5 days per week, for 8 or 12 weeks, as previously described. 1-9 In some longer experiments, mice

exposed to CS for 8 weeks were rested for the final 4 weeks of the experiment to model smoking

cessation. Twice per week, soiled bedding from air-exposed mice was mixed with clean bedding

(1:2 ratio) and transferred to the cages of smoke-exposed mice. Conversely, the soiled bedding

from 12-week CS-exposed mice was mixed with clean bedding and transferred to the cages of air-

exposed mice (Fig S1). Control groups (without FMT) received their own soiled bedding mixed

with clean bedding. Feces were collected weekly, with at least 3 fresh fecal pellets collected and

stored at -80°C until processing.

161 For FMT by oral gavage, fresh feces were collected from normal air-exposed mice and placed

immediately in phosphate buffered saline (PBS) with 0.05% L-cysteine to preserve anaerobic

bacteria (100mg/1.5mL). Feces was gently homogenized by hand and debris removed by

centrifugation (800xg, 3 min). Resulting supernatants were administered by oral gavage, beginning

in the first week of smoke exposure.

167 For antibiotic depletion experiments, mice were not exposed to CS to assess the direct impacts of

168 CS-associated microbiota. Mice received antibiotics (ampicillin, metronidazole, neomycin,

gentamicin [1g/L] and vancomycin [0.5g/L]) in drinking water for 7 days. ¹⁰ Antibiotics were

170 removed and mice received FMT from a separate cohort of air- or CS-exposed donors four times

171 in 10 days.

174

175

176 177 178

179

180 181

182

183

184

185

186

187

188

189

190

191

192

193

194 195

196

197

198 199

200

201

For diet studies, mice were fed a conventional semi-pure diet (AIN93G) or a resistant starch diet (SF11-025; Specialty Feeds, WA, Australia) *ad libitum* commencing 2 week prior to CS-exposure and maintained until the end of experiment. All experiments were approved by University of Newcastle Animal Ethics Committee.

DNA extraction and metagenome assembly and binning

DNA was extracted from 50-100 mg of fecal material using an initial bead beating step and extraction using a Maxwell 16 Research Instrument and Tissue DNA Kit (Promega, USA) according to the manufacturer's protocol. DNA concentrations were measured using a Qubit assay (Life Technologies, USA) and were adjusted to a concentration of 5 ng/ul. Library preparation was performed using Nextera DNA Library Preparation Kits (Illumina, USA) and samples sequenced across two runs on an Illumina NextSeq500 instrument generating an average of 3 Gbp of 150 bp paired-end reads per sample. Each sample was included on both sequencing runs and data combined. Contaminating host reads were removed by mapping against the mouse genome (Mus musculus GRCm38.p5) using BWA v0.7.12¹¹ requiring a minimum alignment length of 30 bases and maximum of 15 clipped bases for reads to be considered of mouse origin. Raw host-free reads from each sample were assembled using Spades v3.12.0¹² with the --meta flag. Reads were mapped to each resulting assembly using BamM v1.7.3 (https://github.com/ecogenomics/BamM) and bins produced using Metabat v2.12.1, 13 MaxBin 14 and GroopM2 v2.0.0-115 implemented within the ensemble binning tool UniteM v0.0.15 (https://github.com/dparks1134/UniteM). Contamination and completeness of bins from all samples were assessed using CheckM v1.0.11.16 Bins with completeness >80% and contamination <7% were retained and de-replicated using dRep v2.05¹⁷ with default settings (99% identity), skipping quality filtering, to produce the final set of metagenome-assembled genomes (MAG). Taxonomy was determined using GTDB-Tk v0.3.0 and v1.5.0¹⁸ with GTDB releases 04-RS89 and 06-RS202.¹⁹ EukDetect v2022²⁰ and MetaPhlAn v3.01 (database v31 CHOCOPhlAn 201901)²¹ were used to detect fungi and viruses (MetaPhlAn only) within metagenomic samples. In addition, raw reads were mapped to fungal and viral reference genomes from NCBI using CoverM v0.6.1 (https://github.com/wwood/CoverM) filtering for alignments ≥95% identity across ≥90% of the read length and genomes with a covered fraction

≥10%. For fungi, all complete or chromosome level genomes were included (247 genomes). For
 viruses, only genomes with host Mus musculus were included (37 genomes).

Metagenomic community profiling

Reads for each sample were mapped to a de-replicated set of 18,342 genomes from NCBI (GTDB release 03-RS83) using BamM with minimum seed length of 25. Genomes with >1x coverage of >1% of the genome and overall coverage of 0.01X, as determined using Mosdepth v0.2.3,²² were retained and combined with a de-replicated set of recovered MAGs for assessment of community composition. Read counts for the final genome set was determined for each sample *via* mapping using BamM with a minimum seed length of 25 bases and filtering for minimum mapping percentage identity of 95%. Per genome read counts were scaled to account for genome size whilst maintaining the raw unmapped read percentage for each sample as a reflection of unrepresented diversity. Relative abundance was calculated using scaled read counts as a fraction of total non-host reads per sample. α-diversity was calculated using QIIME v1.8.0²³ with read counts pergenome normalised to account for library size using DESeq2 v1.20.0.²⁴

Statistical analysis of metagenomic data

Principal component analysis was performed using the R package vegan v2.5-1²⁵ on data transformed using log cumulative-sum-scaling (log-CSS) implemented within metagenomeSeq v1.22.0.²⁶ Differential abundance between sample groups was determined using DESeq2 using read counts per genome scaled to account for genome size and Benjamini-Hochberg adjustment for multiple comparisons. sPLS-DA analysis was conducted using the R package mixOmics v6.3.2²⁷ with centered log-ratio transformed relative abundance (adding pseudo count one order of magnitude below the lowest non-zero value values) with 50x4-fold cross-validation. Host phenotypes were tested for association with microbiome composition using the envfit function based on NMDS ordination of Bray-Curtis distances calculated using the metaMDS function, both implemented within the vegan R package. Significance was determined based on 10,001 permutations and resulting P values were adjusted for multiple comparisons using the Benjamini-Hochberg method. Samples with missing scores were removed. Spearman's rho was calculated using the 'corr.test' function within the R package psych v1.8.12²⁸ based on centered log ratio transformed genome relative abundance and raw phenotypic data. Correlation matrix was

- produced using the 'corrplot' function with the R package corrplot v0.84.²⁹ Non-random relationships between bacteria were identified using the CoNET Cytoscape application.³⁰ Rare taxa (occurrence in <25% of samples) were filtered to avoid spurious relationships, and relationships identified from Pearson and Spearman correlations, mutual similarity, and Kullback-Leibler and Bray-Curtis dissimilarity measures. P-values were combined using Brown's method and adjusted for multiple comparisons using the Benjamini-Hochberg method.
- 239240

Culture of CS extract:

- 241 CS extract was produced by bubbling smoke from one cigarette through 10mL water or PBS. CS
- extract (100μL) was cultured on Yeast Casitone Fatty Acids agar plates in a DG250 anaerobic
- 243 chamber (Don Whitley Scientific) for 48hrs, or analyzed by 16S rRNA amplicon community
- 244 profiling.
- 245

257

246 Assessment of experimental COPD: airway inflammation, emphysema-like alveolar

- 247 enlargement
- 248 Airway inflammation was quantified by total and differential enumeration of immune cells in
- BALF as previously described.^{1, 2, 7} Briefly, two 0.4 ml washes with PBS of the left lung were
- 250 performed, red blood cells lysed and total inflammatory cells counted, cytospun, air dried and
- 251 stained with May-Grunwald-Giemsa for differential counts. For histological analysis, lung tissue
- was perfused with saline via cardiac puncture, inflated (500µL) and fixed in formalin prior to
- 253 mounting, sectioning and staining. Hematoxylin and eosin-stained lung sections were used to
- assess parenchymal inflammation by counting the number of inflammatory cells in 10 randomised
- 255 fields of view at 100x magnification, ^{1, 7, 8} and emphysema-like alveolar enlargement using the
- 256 mean linear intercept, with assessor blinded to sample identity.^{7,31}
- 258 Lung function
- 259 Mice were anaesthetized with ketamine (100 mg/kg) and xylazine (10 mg/kg). Tracheotomy was
- 260 performed, and mice cannulated. A BioSystem Forced Maneuvers (Buxco, Wilminton, NC) and a
- 261 flexivent apparatus (Legacy System, SCIREQ, Montreal, Canada) were used to measure all lung
- 262 function parameters. Each perturbation was conducted a minimum of three times and the average
- 263 calculated for each mouse.^{2, 4, 7-9, 31}

265

270271

278279

293

Colon histopathology

- For histological analysis, colon and ileum tissue was fixed in formalin prior to mounting,
- sectioning, and staining with H&E. Images were taken at 20x magnification and sub-mucosal
- 268 fragmentation area measured using ImageJ software. Blood vessels were enumerated along the
- entire colon and corrected for sub-mucosal length.³¹
 - RNA extraction, cDNA synthesis, and qPCR analysis
- 272 Colon tissues were snap frozen and stored at 80°C. RNA was extracted using a previously
- 273 described TRIzol (ThermoFisher Scientific) protocol utilizing phase separation in chloroform and
- 274 RNA precipitation in isopropanol.^{2, 7, 8, 32} Random-primed reverse transcriptions were performed
- 275 followed by real-time qPCRs with SYBR-green-based detection using a Viia 7 Real Time PCR
- 276 system.^{2, 7, 8, 32} Specific mRNA transcripts were assessed and expressed as relative abundance
- 277 compared to β-actin (*Actb*) expression (Table S18).
 - CyTOF analysis
- 280 For time-of-flight mass cytometry, whole blood was collected into ethylenediaminetetraacetic acid
- 281 (EDTA)-coated tubes and spleen tissue disaggregated using a 70µm cell strainer. Bone marrow
- was collected and immediately incubated with the cell cycle marker iododeoxyuridine (IdU;
- 283 10μM, 1hr, 37°C). For all samples, red blood cells were lysed and cells quantified using trypan
- blue. Single-cell suspensions were stained with the viability marker cisplatin (5µM, 5 minutes,
- room temperature), quenched (5% foetal calf serum, 5mM EDTA in PBS) and collected by
- centrifugation (300xg, 3 minutes, 4°C). Fc receptors were blocked with metal conjugated anti-
- 287 mouse CD16/32 antibody (Table S19, 30 min, 4°C) and quenched before staining with surface
- antibodies (Table S18, 30 min, 4°C). Cells were washed and fixed (4% paraformaldehyde, 4°C
- overnight) before permeabilization in methanol (10 minutes, 4°C), washing and staining with
- 290 intracellular antibodies (Table S19, 45 minutes, room temperature). Samples were washed thrice
- 291 in permeabilization buffer (Thermo Fisher) and stored in 4% paraformaldehyde at 4°C until
- analysis using a Helios instrument (Fluidigm).

296

297

298

299

300

301

302

303

304

305

306

307

308

309

310 311

319 320 The expression levels of 38 markers (Table S19) measured by CyTOF was used as input for downstream analysis. Before analysis, a maximum of 10,000 cells for each sample were randomly selected. Protein expression was transformed with a logicle transformation³³ (width=0.25, top=16,409, full width=4.5) and used for Uniform Manifold Approximation and Projection for Dimension Reduction (UMAP) calculated using the naïve R implementation (umap 0.2.7) of the algorithm with the following settings: number of neighbors=15, number of components=2, distance metric=Euclidean, minimum distance=0.2. Cells clusters showing similar marker expression were calculated according to the Phenograph algorithm (Rphenograph, Github JinmiaoChenLab v. 0.99.1)³⁴ with standard setting and number of nearest neighbors (k)=60. Data were visualized according to the coordinate on the UMAP dimensions and the cluster assignment of each cell. Confusion matrices were calculated normalizing the number of cells in each experimental group to 1,000 and calculating the contribution of each condition in each cluster to avoid bias from different cell numbers in experimental groups. Finally, a heatmap was generated using the mean marker expression in each cluster scaled for visualization. Data were visualized using the R packages ggplot2 (v. 3.3.2) and pheatmap (v. 1.0.12). All analysis was performed in a dockerized environment based on R 4.0.3 and Bioconductor 3.12 (lorenzobonaguro/flowtools:v2).

Cell culture

- Raw 264.7 monocytes (1x10⁶) were seeded into 12-well plates and allowed to adhere overnight. 312
- Feces from CS- or air-exposed mice were homogenized in DMEM (100mg/mL) and sterile-313
- 314 filtered. Cells were incubated in media alone, or 1:1,000 dilutions of filtered fecal homogenate for
- 315 24 hours. During the final 4 hours of incubation lipopolysaccharide (1µg/mL), monophosphoryl
- 316
- lipid A (4µg/mL), lipoteichoic acid (1µg/mL) or dimethyl sulfoxide (0.5%) were added to cell
- 317 media. Media was collected and stored at -80°C until TNFα protein was assessed using Duoset
- 318 ELISA kits (R & D Systems).

Flow cytometry

- 321 Excised colons with contents removed were cut into 1cm pieces, placed in pre-digestion buffer
- 322 (2mM EDTA in Hanks buffered salt solution [HBSS]), and incubated with shaking (150 rpm, 15
- 323 min, 37°C). Tissues were washed thrice in HBSS buffer before incubation in digestion buffer

- 324 (0.425mg/ml Collagenase V, 0.625mg/ml Collagenase D, 1mg/ml Dispase II [Sigma], 10% FBS
- in RPMI 1640; 150 rpm, 45 minutes, 37°C). Digested tissue was passed through a 100μm cell
- 326 strainer, centrifuged (1500 rpm, 7 min, 4°C) and resuspended in FACS buffer (2% FBS, 2mM
- 327 EDTA in PBS) for staining.
- Lung tissue was stored in HEPES buffer (10mM HEPES-NaOH pH 7.4;150 mM NaCl; 5mM KCl;
- 329 1mM MgCl₂; 1.8mM CaCl₂) containing Collagenase D (40U/mL, Sigma-Aldrich) and DNase 1
- 330 (2mg/mL, Sigma-Aldrich) and mechanically disrupted using a gentleMacs machine (m1 lung
- program, Miltenyl Biotec, NSW Australia). After incubation (150 rpm, 20 min, 37°C), tissues were
- disrupted again using the gentleMAcs machine (m2_lung program), strained using a 100µm cell
- strainer, and collected by centrifugation (1500 rpm, 5 min, 4°C). Red blood cells were lysed using
- 334 red blood cell lysis buffer (5 min, 4 °C) before inactivation in FACS buffer, centrifugation and
- 335 resuspension in FACS buffer.

- Single cell isolations $(1x10^6)$ were collected by centrifuged $(1500 \text{ rpm}, 7 \text{ min}, 4^{\circ}\text{C})$, washed with
- 337 PBS, and stained with viability dye (Table S19; 30 min, 4°C). Cells were washed with FACS
- buffer, Fc receptors blocked (BD Biosciences, 15 min, 4°C), and stained with antibodies (Table
- 339 S20, 30 min, 4°C). Stained cells were washed three times with FACS buffer before analysis using
- an LSR Fortessa cytometer (BD Biosciences) and FlowJo software (TreeStar).

DNA extraction and 16S rRNA amplicon community profiling

- DNA was extracted from fecal samples using the PowerSoil DNA extraction kit according to the
- manufacturer's instructions (MoBio, Carlsbad, California). For community profiling, the V5-V8
- region of the 16S rRNA gene was amplified using a modified two-step PCR protocol.³⁵ The first
- 346 round 50μl reaction mixture comprised 20ng of template DNA, molecular biology grade water,
- 347 5ul 10x PCR buffer (Fisher Scientific), 4ul of 25mM MgCl2 (Fisher Scientific), 1.5ul BSA (New
- England Biolabs), 1µl of 10mM dNTPmix (Fisher Scientific), 1µl of 10nM forward primer 803F
- 349 (803Fa-5': TTAGATACCCTGGTAGTC; 803Fb-5': TTAGATACCCSGGTAGTC; 803Fc-5':
- 350 TTAGATACCCYHGTAGTC; 803Fd-5': TTAGAGACCCYGGTAGTC; mixed at ratios of
- 351 (2a:b:c:d), 1 μl of 10nM reverse primer 1392wR (ACGGGCGGTGWGTRC)) and 0.2μl of 5U/ul
- 352 Taq Polymerase (Fisher Scientific). Cycling conditions were as follows: 95°C for 3 minutes, 30
- 353 cycles of 95°C for 30 seconds, 55°C for 30 seconds and 74°C for 30 seconds followed by a final
- extension of 74°C for 10 minutes. PCR products were re-amplified in a second reaction using

- primers containing (5'-3') 454 adaptor sequences, barcode (only for reverse primer), linker
- sequence and the gene-specific primer sequence (803F and 1392wR: pyroLSSU803F -
- 357 CCTATCCCCTGTGTGCCTTGGCAGTCTCAGTTAGAKACCCBNGTAGTC
- 358 pyroLSSU1392wR
- 359 CCATCTCATCCCTGCGTGTCTCCGACTCAGACATAGTACGGGCGGTGWGTRC). For
- 360 the second step reactions, 2 μl of the first step PCR product was added as template to a 50 μl
- 361 reaction. PCR conditions were the same as those for the first step with the number of cycles
- 362 reduced to 10. Amplicons were purified using AMPure beads (Beckman Coulter) and pooled in
- equal ratios. Amplicon pools were sequenced from the reverse primer using 454 GS-FLX Titanium
- 364 chemistry.

373374

- Amplicon sequences were demultiplexed and converted to fastq files using QIIME v1.9.1 scripts
- 367 split libraries.py, convert fastaqual fastq.py and split sequence file on sample ids.py. Reads
- 368 were then quality filtered and trimmed of adapter sequence using BBMap v38.41
- 369 (https://sourceforge.net/projects/bbmap/ via BBDuk; ktrim=l k=15 mink=10 hdist=1 interleaved=f
- 370 copyundefined=t mm=f qtrim=rl trimq=10 minlen=400). Sequence variants were defined using
- 371 QIIME2 v2019.10³⁶ and DADA2 (via denoise-pyro).³⁷ Taxonomy was assigned using QIIME2
- feature-classifier ³⁸ classify-consensus-blast against the Silva v138 database. ³⁹

Proteomics of mouse feces

- Feces (100µg) were added to 500µL of sodium bicarbonate, vortexed with 2.5-mm glass beads
- and supernatants collected (300xg, 5 min, 4°C). Pellets were resuspended in sodium bicarbonate,
- 377 centrifuged and supernatants collected a further two times. Supernatants were combined and
- washes repeated to remove debris before final cell collection (14,000xg, 20 min, 4°C). Cells were
- 379 aliquoted (~30mg wet weight per aliquot) and subjected to enzymatic degradation (20μL lysozyme
- 380 in buffer containing 20mM TrisHCl, 2 mM EDTA and 1% Triton X-100; 30 min, 37°C).
- 381 Incubation was halted with sodium bicarbonate and cell debris removed by centrifugation
- 382 (12,000xg, 20 min, 4°C). Proteins (150μg) were precipitated, resuspended in 8M urea, reduced
- with dithiothreitol and alkylated with iodoacetamide. Samples were diluted in 50mM ammonium
- 384 bicarbonate to a final urea concentration of 1M and digested overnight with trypsin (50:1
- protein:enzyme, 37°C). Following acidification in 1% trifluoroacetic acid, 20µg of peptides were

388 389

390

391 392

393

394

395

396

397

398

399

400 401

402 403

404

405 406

407 408 409

410 411

412

413

414

415

416

dried by vacuum concentration, resuspended in 2% acetonitrile/0.1% trifluoroacetic acid and 500ng injected onto a trapping column for pre-concentration (Acclaim Pepmap100, 20x0.075mm, 3µm C18, Thermo Scientific), followed by nanoflow liquid chromatography (Ultimate 3000RSLCnano, Thermo Scientific). Peptide separation was achieved over a 250x0.075 mm ID, PepMap 2µm EasySpray C18 column using the following mobile phases: water, 0.1% formic acid (solvent A) and 80% acetonitrile incorporating 0.1% formic acid (solvent B). Peptides were resolved using a linear gradient from 2% B to 35% B over 70 min at a constant flow of 300nl/min. Peptides were introduced via an EasySpray Nano source coupled to a Q-Exactive Plus Quadrupole Orbitrap mass spectrometer (Thermo Scientific) and subjected to data dependent tandem mass spectrometry (MS/MS) using the following parameters. Full MS scans were acquired in profile mode, positive polarity at a resolution of 70,000, automatic gain control target 1x10⁶ and a max injection time of 50ms. Data dependent MS/MS was then preformed at a resolution of 17,500 on the top 20 ions with a charge ≥ 2 , automatic gain control target of $5x10^5$, max injection time of 120ms, using a stepped NCE of 26 and 30. Dynamic exclusion was set at 15 seconds. .raw files were processed in Proteome Discoverer v2.1 using the Sequest HT algorithm 40 and searched against the mouse gut microbiota GigaDB database.⁴¹

Integration of proteomics and metagenomics

Metagenomics results were collapsed by adding relative abundances of bacteria from the same genera. Genera and proteins present in \geq 50% of samples were included for analysis. Both microbiome and proteomic data were integrated through correlation analysis using the psych package in R^{42} and Diablo mixOmics package.

Metabolomics

Caecum contents were collected from mice exposed to CS or normal air for 12 weeks, snap frozen and shipped on dry ice to Metabolon Inc (Durham, NC). Samples were analysed using the Global HD4 mass spectrometry platform using ultra-high performance liquid chromatography. Peaks were identified by comparison to a library of purified standards (or recurrent unknown compounds) containing retention time/index, mass:charge ratio (m/z), and chromatographic data (including MS/MS spectral data), and the relative abundance of each metabolite scaled such that the median value was equal to 1.

418

419

420

421 422

Supplementary References:

- Beckett EL, Stevens RL, Jarnicki AG, Kim RY, Hanish I, Hansbro NG, et al. A new short-term mouse model of chronic obstructive pulmonary disease identifies a role for mast cell tryptase in pathogenesis. J Allergy Clin Immunol 2013;**131**:752-62.
- Starkey MR, Plank MW, Casolari P, Papi A, Pavlidis S, Guo Y, et al. IL-22 and its receptors are increased in human and experimental COPD and contribute to pathogenesis. Eur Respir J 2019;**54**.
- 429 3 Prihandoko R, Kaur D, Wiegman CH, Alvarez-Curto E, Donovan C, Chachi L, et al. 430 Pathophysiological regulation of lung function by the free fatty acid receptor FFA4. Sci Transl Med 431 2020:**12**.
- 432 4 Schanin J, Gebremeskel S, Korver W, Falahati R, Butuci M, Haw TJ, et al. A monoclonal 433 antibody to Siglec-8 suppresses non-allergic airway inflammation and inhibits IgE-independent 434 mast cell activation. Mucosal Immunol 2021;**14**:366-76.
- Cooper GE, Mayall J, Donovan C, Haw TJ, Budden KF, Hansbro NG, *et al.* Antiviral Responses of Tissue-resident CD49a(+) Lung Natural Killer Cells Are Dysregulated in Chronic Obstructive Pulmonary Disease. Am J Respir Crit Care Med 2023;**207**:553-65.
- 438 6 Tu X, Kim RY, Brown AC, de Jong E, Jones-Freeman B, Ali MK, et al. Airway and parenchymal transcriptomics in a novel model of asthma and COPD overlap. J Allergy Clin Immunol 2022;**150**:817-29.e6.
- Haw TJ, Starkey MR, Pavlidis S, Fricker M, Arthurs AL, Nair PM, et al. Toll-like receptor 2 and 4 have opposing roles in the pathogenesis of cigarette smoke-induced chronic obstructive pulmonary disease. Am J Physiol Lung Cell Mol Physiol 2018;**314**:L298-l317.
- 444 8 Lu Z, Van Eeckhoutte HP, Liu G, Nair PM, Jones B, Gillis CM, et al. Necroptosis Signalling 445 Promotes Inflammation, Airway Remodelling and Emphysema in COPD. Am J Respir Crit Care Med 446 2021.
- 9 Skerrett-Byrne DA, Bromfield EG, Murray HC, Jamaluddin MFB, Jarnicki AG, Fricker M, et 448 al. Time-resolved proteomic profiling of cigarette smoke-induced experimental chronic 449 obstructive pulmonary disease. Respirology 2021.
- 450 10 Scott NA, Andrusaite A, Andersen P, Lawson M, Alcon-Giner C, Leclaire C, et al. Antibiotics 451 induce sustained dysregulation of intestinal T cell immunity by perturbing macrophage 452 homeostasis. Sci Transl Med 2018;**10**.
- 453 11 Li H, Durbin R. Fast and accurate short read alignment with Burrows-Wheeler transform.
- 454 Bioinformatics 2009;**25**:1754-60.
- Nurk S, Meleshko D, Korobeynikov A, Pevzner PA. metaSPAdes: a new versatile metagenomic assembler. Genome Research 2017;**27**:824-34.

- 457 13 Kang DD, Froula J, Egan R, Wang Z. MetaBAT, an efficient tool for accurately
- reconstructing single genomes from complex microbial communities. PeerJ 2015;**3**:e1165.
- 459 14 Wu Y-W, Tang Y-H, Tringe SG, Simmons BA, Singer SW. MaxBin: an automated binning
- method to recover individual genomes from metagenomes using an expectation-maximization
- algorithm. Microbiome 2014;**2**:26.
- 462 15 Imelfort M, Parks D, Woodcroft BJ, Dennis P, Hugenholtz P, Tyson GW. GroopM: an
- automated tool for the recovery of population genomes from related metagenomes. PeerJ. San
- 464 Francisco, USA: PeerJ Inc., 2014:e603.
- Parks DH, Imelfort M, Skennerton CT, Hugenholtz P, Tyson GW. CheckM: assessing the
- 466 quality of microbial genomes recovered from isolates, single cells, and metagenomes. Genome
- 467 Research 2015;**25**:1043-55.
- 468 17 Olm MR, Brown CT, Brooks B, Banfield JF. dRep: a tool for fast and accurate genomic
- 469 comparisons that enables improved genome recovery from metagenomes through de-
- 470 replication. Isme Journal 2017;**11**:2864-8.
- 471 18 Chaumeil P-A, Mussig AJ, Hugenholtz P, Parks DH. GTDB-Tk: a toolkit to classify genomes
- with the Genome Taxonomy Database. Bioinformatics 2019;**36**:1925-7.
- 473 19 Parks DH, Chuvochina M, Chaumeil P-A, Rinke C, Mussig AJ, Hugenholtz P. A complete
- domain-to-species taxonomy for Bacteria and Archaea. Nature Biotechnology 2020.
- Lind AL, Pollard KS. Accurate and sensitive detection of microbial eukaryotes from whole
- 476 metagenome shotgun sequencing. Microbiome 2021;**9**:58.
- 477 21 Truong DT, Franzosa EA, Tickle TL, Scholz M, Weingart G, Pasolli E, et al. MetaPhlAn2 for
- 478 enhanced metagenomic taxonomic profiling. Nat Methods 2015;12:902-3.
- 479 22 Pedersen BS, Quinlan AR. Mosdepth: quick coverage calculation for genomes and
- 480 exomes. Bioinformatics 2018;34:867-8.
- 481 23 Caporaso JG, Kuczynski J, Stombaugh J, Bittinger K, Bushman FD, Costello EK, et al. QIIME
- allows analysis of high-throughput community sequencing data. Nature methods 2010;7:335-6.
- 483 24 Love MI, Huber W, Anders S. Moderated estimation of fold change and dispersion for
- 484 RNA-seq data with DESeq2. Genome biology 2014;15:550.
- 485 25 Oksanen J, Blanchet FG, Kindt R, Legendre P, Minchin PR, O'Hara RB, et al. vegan:
- 486 Community Ecology Package. R package version 23-1, 2015.
- 487 26 Paulson JN, Stine OC, Bravo HC, Pop M. Differential abundance analysis for microbial
- 488 marker-gene surveys. Nature methods 2013;10:1200-2.
- 489 27 Rohart F, Gautier B, Singh A, Lê Cao K-A. mixOmics: An R package for 'omics feature
- 490 selection and multiple data integration. PLOS Computational Biology 2017;13:e1005752.
- 491 28 Revelle W. psych: Procedures for Personality and Psychological Research. R package
- 492 version 1812, 2018.
- 493 29 Wei T, Simko V. corrplot: Visualization of a Correlation Matrix. R package version 084,
- 494 2018.
- 495 30 Faust K, Raes J. CoNet app: inference of biological association networks using Cytoscape.
- 496 F1000Res 2016;**5**:1519.
- 497 31 Fricker M, Goggins BJ, Mateer S, Jones B, Kim RY, Gellatly SL, et al. Chronic cigarette smoke
- 498 exposure induces systemic hypoxia that drives intestinal dysfunction. JCI Insight 2018;3.

- 499 32 Budden KF, Gellatly SL, Vaughan A, Amorim N, Horvat JC, Hansbro NG, et al. Probiotic
- 500 Bifidobacterium longum subsp. longum Protects against Cigarette Smoke-Induced Inflammation
- 501 in Mice. Int J Mol Sci 2022;**24**.
- 502 33 Parks DR, Roederer M, Moore WA. A new "Logicle" display method avoids deceptive
- effects of logarithmic scaling for low signals and compensated data. Cytometry A 2006;69:541-
- 504 51.
- 505 34 Levine JH, Simonds EF, Bendall SC, Davis KL, Amir el AD, Tadmor MD, et al. Data-Driven
- 506 Phenotypic Dissection of AML Reveals Progenitor-like Cells that Correlate with Prognosis. Cell
- 507 2015;**162**:184-97.
- Berry D, Ben Mahfoudh K, Wagner M, Loy A. Barcoded primers used in multiplex amplicon
- pyrosequencing bias amplification. Appl Environ Microbiol 2011;**77**:7846-9.
- 510 36 Bolyen E, Rideout JR, Dillon MR, Bokulich NA, Abnet CC, Al-Ghalith GA, et al. Reproducible,
- 511 interactive, scalable and extensible microbiome data science using QIIME 2. Nat Biotechnol
- 512 2019;**37**:852-7.
- 513 37 Callahan BJ, McMurdie PJ, Rosen MJ, Han AW, Johnson AJ, Holmes SP. DADA2: High-
- resolution sample inference from Illumina amplicon data. Nat Methods 2016;**13**:581-3.
- 515 38 Bokulich NA, Kaehler BD, Rideout JR, Dillon M, Bolyen E, Knight R, et al. Optimizing
- 516 taxonomic classification of marker-gene amplicon sequences with QIIME 2's q2-feature-classifier
- 517 plugin. Microbiome 2018;**6**:90.
- 39 Quast C, Pruesse E, Yilmaz P, Gerken J, Schweer T, Yarza P, et al. The SILVA ribosomal RNA
- 519 gene database project: improved data processing and web-based tools. Nucleic Acids Res
- 520 2013;**41**:D590-6.
- 521 40 Washburn MP. The H-index of 'an approach to correlate tandem mass spectral data of
- 522 peptides with amino acid sequences in a protein database'. J Am Soc Mass Spectrom
- 523 2015;**26**:1799-803.

- 524 41 Xiao L, Feng Q, Liang S, Sonne SB, Xia Z, Qiu X, et al. A catalog of the mouse gut
- 525 metagenome. Nat Biotechnol 2015;33:1103-8.
- Revelle W. psych: Procedures for Psychological, Psychometric, and Personality Research.
- 527 Northwestern University, 2021.